# The ULK1-FBXW5-SEC23B nexus controls autophagy

Yeon-Tae Jeong[1,2], Daniele Simoneschi[1,2], Sarah Keegan[1,2,3], David Melville[4], Natalia S. Adler[5], Anita Saraf[6], Laurence Florens[6], Michael P. Washburn[6,7], Claudio N. Cavasotto[5], David Fenyö[1,2,3], Ana-Maria Cuervo[8], Mario Rossi[1,2,5], and Michele Pagano[1,2,9*]

[1]Department of Biochemistry and Molecular Pharmacology, [2]Perlmutter NYU Cancer Center, [3]Institute for System Genetics, and [9]Howard Hughes Medical Institute; New York University School of Medicine, 522 First Avenue, New York, NY 10016, USA. [4]Department of Molecular and Cellular Biology and Howard Hughes Medical Institute, University of California, Berkeley, CA, USA. [5]Instituto de Investigación en Biomedicina de Buenos Aires-CONICET--Partner Institute of the Max Planck Society, C1425FQD Buenos Aires, Argentina. [6]The Stowers Institute for Medical Research, 1000 East 50th Street, Kansas City, MO 64110, USA. [7]Department of Pathology and Laboratory Medicine, The University of Kansas Medical Center, 3901 Rainbow Boulevard, Kansas City, Kansas 66160, USA. [8]Department of Developmental and Molecular Biology and Institute for Aging Studies, Albert Einstein College of Medicine, Bronx, NY USA.

*Correspondence: michele.pagano@nyumc.org

**ABSTRACT**

In response to nutrient deprivation, the cell needs to mobilize an extensive amount of membrane to form and grow the autophagosome, allowing the progression of autophagy. By providing membranes and a source for LC3 lipidation, COPII (Coat Protein Complex II) localizes to the endoplasmic reticulum (ER)-Golgi intermediate compartment (ERGIC) and promotes autophagosome biogenesis. However, the molecular mechanisms that, in response to starvation, divert COPII from the secretory pathway to the autophagic pathway are largely unknown. Here, we show that the F-box protein FBXW5 targets SEC23B, a component of COPII, for proteasomal degradation and that this event limits the autophagic flux in the presence of nutrients. In response to starvation, ULK1 phosphorylates SEC23B on Serine 186, preventing the interaction of SEC23B with FBXW5 and, therefore, inhibiting its degradation. Phosphorylated and stabilized SEC23B associates with SEC24A and SEC24B, but not SEC24C and SEC24D, and they re-localize to the ERGIC, promoting autophagic flux. Induction of autophagy and localization of both SEC23B and SEC24B to the ERGIC in response to nutrient deprivation are significantly reduced in SEC23B(S186A) knock-in cells. We propose that, in the presence of nutrients, FBXW5 limits COPII-mediated autophagosome biogenesis. Inhibition of this event by ULK1 ensures efficient execution of the autophagic cascade in response to nutrient starvation.

## INTRODUCTION

Macro-autophagy (more commonly referred to as autophagy) is a highly conserved process present in all eukaryotes, which allows the degradation of proteins and organelles by lysosomes (Hurley and Young, 2017; Klionsky et al., 2016; Lamb et al., 2013). It is characterized by the formation of the double-membraned autophagosome that transports cytoplasmic cargos to lysosomes, where the autophagic cargo is subjected to degradation. In a simplistic way, autophagy can be classified into "basal" and "induced." The former is used to maintain cellular homeostasis by promoting the turnover of cytoplasmic components, and the latter is part of the cellular response to stressors (*e.g.,* to produce amino acids upon nutrient deprivation). Due to its role in many cellular processes, it is not surprising that deregulation of autophagy plays a role in many human diseases, such as neurodegenerative disorders, cancer, and infection (Jiang and Mizushima, 2014; Rybstein et al., 2018).

The UNC51-like kinase 1 [ULK1, AKA autophagy-related (ATG) protein ATG1] is a master regulator of autophagy (Dankert et al., 2016; Hurley and Young, 2017; Lamb et al., 2013; Mizushima, 2010). Specifically, in response to nutrient starvation or mTOR inhibition, ULK1 is activated and, in turn, this leads to enhanced activity of the autophagy-specific class III phosphoinositide 3-kinase (PI3KC3) complex, which is comprised of VPS34 (AKA PIK3C3), p150 (AKA VPS15 and PIK3R4), BECLIN-1 (AKA ATG6), and ATG14 (Hurley and Young, 2017; Lamb et al., 2013). The activation of the PI3KC3 complex results in the production of PI(3)P (phosphatidylinositol 3-phosphate), which is necessary for the recruitment of downstream effectors and the subsequent nucleation of the autophagosome. Next, two consecutive ubiquitylation-like reactions catalyzed by certain ATG proteins mediate the attachment of phosphatidylethanolamine to LC3 family proteins (commonly referred to as LC3 lipidation), promoting the expansion and closure of the

autophagosome (Mizushima et al., 2011). Originally, it was thought that the autophagosome only derives from mobile cytoplasmic vesicles characterized by the transmembrane protein ATG9, which are recruited to the ER. However, it has become clear that, in response to starvation, additional sources of membrane are necessary for the formation and growth of the autophagosome (Davis et al., 2017; Hurley and Young, 2017; Wang et al., 2014).

The coat protein complex II (COPII) is a multi-subunit protein complex essential for the transport of cellular cargos from the ER to the Golgi apparatus (Fromme et al., 2008; Zanetti et al., 2011). A key component of COPII is SEC23, whose importance in maintaining cellular homeostasis is highlighted by the fact that mutations in the two SEC23 paralogs (SEC23A and SEC23B) cause the human genetic diseases cranio-lenticulo-sutural dysplasia and congenital dyserythropoietic anemia type II, respectively (Boyadjiev et al., 2006; Lang et al., 2006; Schwarz et al., 2009). The other components of COPII are SEC13, SEC24, SEC31, and SAR1.

COPII vesicles emerge from specialized domains of the ER called ER exit sites (ERES) (Zanetti et al., 2011). However, in response to starvation, when the secretory pathway is inhibited (Wang et al., 2014; Zacharogianni et al., 2014; Zacharogianni et al., 2011) and there is an urgent need for membranes to form autophagosomes, ERES enlarge and patches along the ERGIC to function in autophagosome biogenesis (Davis et al., 2017; Egan et al., 2015; Ge et al., 2017; Ge et al., 2014; Hurley and Young, 2017; Sanchez-Wandelmer et al., 2015). In mammals, disruption of ERES inhibits autophagosome biogenesis at an early stage (Stadel et al., 2015; Zoppino et al., 2010). Moreover, in response to nutrient starvation, the PI3KC3 complex, which is activated by ULK1, promotes the recruitment of COPII components to the ERGIC (Egan et al., 2015; Ge et al., 2013; Ge et al., 2014;

Karanasios et al., 2016). Next, specialized COPII vesicles budding from the ERGIC act as precursors for LC3 lipidation, a critical step in autophagosome biogenesis (Egan et al., 2015; Ge et al., 2017; Ge et al., 2014). The functions of COPII in the autophagic pathway are conserved along evolution. In fact, in response to starvation, yeast COPII components physically interact with core elements required for autophagy, and COPII vesicles provide membrane sources for the growing autophagosome (Davis et al., 2016; Ishihara et al., 2001; Lemus et al., 2016; Reggiori et al., 2004; Tan et al., 2013). However, how the components of COPII vesicles are regulated in response to nutrient deprivation to allow their contribution to autophagosome biogenesis is largely unknown.

The ubiquitin-proteasome system is necessary for the precise spatiotemporal degradation of numerous key cellular regulators, and the selectivity of this process is determined by a large family of ubiquitin ligases. SKP1-CUL1-F-box protein (SCF) complexes form a family of multi-subunit ubiquitin ligases, which, in turn, is part of the super-family of Cullin-Ring Ligases (CRLs) (Petroski and Deshaies, 2005; Skaar et al., 2013, 2014). In human, 69 F-box proteins act as the substrate receptor subunits of SCF ubiquitin ligases, allowing the regulation of hundreds of substrate proteins. Thus, SCFs control a multitude of cellular processes whose deregulation is implicated in many pathologies, including cancer (Frescas and Pagano, 2008; Wang et al., 2014).

## RESULTS

### *FBXW5 binds SEC23B and promotes its proteasomal degradation*

To identify $SCF^{FBXW5}$ substrates, Streptag-FLAG (SF)-tagged FBXW5 was transiently expressed in HEK293T cells and affinity purified for analysis by Multidimensional Protein

Identification Technology (MudPIT) (Florens and Washburn, 2006; Jeong et al., 2013). MudPIT revealed the presence of peptides corresponding to SKP1 and CUL1 (as expected), as well as 15 unique peptides derived from the COPII coat subunit SEC23B (http://www.stowers.org/research/publications/libpb-1118). To confirm the binding between SEC23B and FBXW5 and its specificity, we screened a panel of nine human F-box proteins. SF-tagged F-box proteins were expressed in HEK293T cells and affinity precipitated to evaluate their interaction with SEC23B. We found that FBXW5 was the only F-box protein capable of co-precipitating with endogenous SEC23B (Fig. 1A).

Next, we investigated whether SEC23B is targeted for proteolysis by FBXW5. Expression of wild-type FBXW5 resulted in a reduction in the levels of both endogenous and exogenous SEC23B, as detected by immunoblotting or immunofluorescence microscopy (Fig. 1B-C, Supplementary Fig. S1B). This reduction depended on the ability of FBXW5 to form an active SCF complex as demonstrated by the observation that the expression of FBXW5(ΔF), a mutant in which the F-box domain was deleted, did not affect SEC23B protein levels (Fig. 1B). Moreover, either co-expression with dominant negative (DN)-CUL1 (a mutant of CUL1 lacking its C-terminus, which retains the binding to F-box proteins and SKP1, but not to the catalytic subunit RBX1) or addition of MLN4924 (a NEDD8 activating enzyme inhibitor used to inhibit the activity of SCFs) blocked the FBXW5-dependent degradation of SEC23B (Fig. 1C and Fig. 1E). In contrast, although it has been reported that FBXW5 can form a functional $CRL4^{FBXW5}$ complex (Frescas and Pagano, 2008; Kim et al., 2013), co-expression of a CUL4 dominant negative mutant (DN-CUL4) did not interfere with the FBXW5-dependent degradation of SEC23B (Fig. 1C). The observed reduction of SEC23B protein levels upon FBXW5 transfection was rescued also by the addition of the proteasome inhibitor MG132 (Fig. 1C), indicating that the decrease in SEC23B levels was due to proteasome-mediated proteolysis.

To confirm that FBXW5 regulates the degradation of SEC23B, we used RNA interference to reduce FBXW5 expression. Depleting FBXW5 using three different siRNA oligos (each individually) induced an increase in both the steady state-levels and the stability of endogenous SEC23B in two different cell types (Fig. 1D and Supplementary Fig. S1C).

Altogether, these results indicate that FBXW5 controls the proteasome-mediated degradation of SEC23B.

As previously mentioned, SEC23B is a fundamental component of COPII vesicles, and therefore it interacts with several COPII-vesicle proteins (Fromme et al., 2008). Nevertheless, immunopurified FBXW5 does not co-precipitate other COPII vesicle proteins (Fig. 1E and http://www.stowers.org/research/publications/libpb-1118), suggesting that the subpopulation of SEC23B interacting with FBXW5 is not integrated within COPII vesicles. SEC23B and SEC24 proteins form tight heterodimers (Fromme et al., 2008); therefore, we reasoned that FBXW5 and SEC24 proteins might compete for the binding to SEC23B. To examine this possibility, we co-transfected HEK293T cells with FBXW5 and increasing amounts of SEC24B and subjected the resulting lysates to affinity purification. In line with our hypothesis, increasing concentrations of SEC24B resulted in a marked decrease in the binding of endogenous SEC23B to FBXW5 (Fig. 1F). Consistent with an impaired interaction between SEC23B and FBXW5, increasing amounts of SEC24B also induced an increase in the levels of endogenous SEC23B (Fig. 1F). These results support the hypothesis that SEC23B cannot simultaneously bind to FBXW5 and SEC24B, suggesting that these two proteins compete for the same binding region on SEC23B. In agreement with this model, using a panel of SEC23B deletion mutants, we found that the binding to FBXW5 is mediated by the TRUNK domain of SEC23B (Supplementary Fig. S1D-F), which

has been shown to mediate the SEC23-SEC24 interaction (Mancias and Goldberg, 2007). In fact, SEC23B(100-767), a deletion mutant containing the TRUNK domain, was able to co-precipitate endogenous FBXW5, whereas SEC23B(400-767), a mutant missing the TRUNK domain, was not (Supplementary Fig. S1D-F).

Next, we used an immobilized synthetic peptide containing the previously reported SEC24-interacting sequence of SEC23B (a.a. 180-194 in human, see Supplementary Fig. S1D and Supplementary Fig. S1F) (Mancias and Goldberg, 2007) and tested its ability to bind endogenous FBXW5 present in cellular extracts. While the immobilized SEC23B peptide efficiently bound FBXW5, it failed to pull down other F-box proteins (Fig. 1G), suggesting that this 14-amino acid region is sufficient for the binding to FBXW5.

Taken together, these results indicate that FBXW5 and SEC24B associate with SEC23B in a mutually exclusive fashion and may compete for the same binding region in SEC23B.

*ULK1 phosphorylates SEC23B on Serine 186 that is present in the binding motif for FBXW5 and SEC24*

The interactions between most F-box proteins and their cognate substrates are often regulated by post-translational modifications (most often phosphorylation) (Skaar et al., 2013). Therefore, we looked for phosphorylation consensus sequences for known kinases within the FBXW5-binding region of SEC23B and found that Serine 186 (S186) is part of a highly conserved ULK1 phosphorylation motif (Egan et al., 2015) (Supplementary Fig. S2A-B). We first investigated whether S186 is phosphorylated in cells. To this end, we generated a phospho-specific antibody against a peptide (a.a. 180-194) containing phosphorylated Serine at position 186. This antibody specifically detected the

phosphopeptide, but not the unphosphorylated peptide (Supplementary Fig. S2C). Moreover, it recognized both wild-type SEC23B and a SEC23B(S186D) mutant (which mimics Ser186 phosphorylation), but not the SEC23B(S186A) mutant (Supplementary Fig. S2D), providing evidence that SEC23B is phosphorylated *in vivo* on S186.

Next, to test whether Ser186 on SEC23B can serve as a phospho-acceptor for ULK1, we co-expressed FLAG-tagged wild-type SEC23B together with either wild type ULK1 or a kinase-dead (KD) mutant. Only wild-type ULK1 induced the phosphorylation of both endogenous and exogenous SEC23B on S186, as detected with our phospho-specific antibody (Fig. 2A and Supplementary Fig. S2E) (endogenous phosphorylated SEC23B was detected in whole cell extracts, and exogenous phosphorylated SEC23B was detected in both in cell extracts and anti-FLAG immunoprecipitates). In contrast, in cells expressing SEC23B(S186A), only endogenous SEC23B was phosphorylated by ULK1(Fig. 2A and Supplementary Fig. S2E). We further confirmed that SEC23B is an ULK1 substrate by using purified proteins in an *in vitro* phosphorylation assay (Supplementary Fig. S2F). Moreover, addition of a specific ULK1 inhibitor, SBI-0206965, blocked ULK1-dependent phosphorylation of endogenous SEC23B in a dose-dependent manner, similar to what observed for ATG13 (Fig. 2B), a canonical substrate of ULK1.

Next, we studied how nutrient deprivation, a condition that activates ULK1, modulates the phosphorylation of SEC23B on S186. After substituting the growth medium, which contains 10% fetal bovine serum, with Earle's balanced salt solution (EBSS), we observed a time-dependent increase in the phosphorylation of endogenous SEC23B as well as two other known substrates of ULK1, and this phosphorylation was inhibited by treating cells with SBI-0206965 (Fig. 2C and Supplementary Fig. S2G).

We concluded that, in response to starvation, ULK1 phosphorylates SEC23B on S186.

*ULK1-dependent phosphorylation of SEC23B inhibits its interaction with and degradation via FBXW5*

To investigate whether phosphorylation on S186 affects the SEC23B-FBXW5 interaction, we used a phosphorylated version of the synthetic peptide employed for the binding experiments. While the non-phosphorylated peptide efficiently bound FBXW5, as previously observed (Fig. 1G), a corresponding peptide containing phosphorylated Ser186 displayed a strongly reduced ability to bind FBXW5 (Supplementary Fig. S2H). This indicates that Ser186 phosphorylation inhibits the interaction between these two proteins, in agreement with the fact that the binding of FBXW5 to the phospho-mimetic SEC23B(S186D) mutant is abolished, while FBXW5 binding to SEC23B(S186A) is increased (Fig. 2D). Accordingly, endogenous SEC23B phosphorylated on Ser186 was not affinity purified with FBXW5 (Fig. 2E). Similarly, upon nutrient deprivation (when SE23B becomes phosphorylated on Ser186) the interaction between FBXW5 and SEC23B decreased (Supplementary Fig. S2I).

Consistent with the observed impaired interaction with FBXW5, the levels of SEC23B(S186D) did not decrease in the presence of FBXW5 (Fig. 2F) and it exhibited a longer half-life than wild-type SEC23B (Fig. 2G). These results suggest that ULK1 phosphorylates Ser186 in SEC23B, inhibiting its interaction with and degradation via FBXW5. Concurring with this hypothesis, silencing of ULK1, but not ULK2, reduced the levels of SEC23B phosphorylated on Ser186 and induced a decrease in the levels of endogenous SEC23B in starved cells (Fig. 2H and Supplementary Fig. S2J). Moreover, co-silencing FBXW5 rescued the decrease in SEC23B levels induced by the depletion of ULK1

but did not alter the amount of phosphorylated SEC23B (Fig. 2H), confirming that ULK1 and FBXW5 have an antagonistic effect on the control of SEC23B protein abundance.

Significantly, although Ser186 is located at the interface between the SEC23 and SEC24 heterodimer binding region (Mancias and Goldberg, 2007) (Supplementary Fig. S1F) and its phosphorylation blocks the SEC23B-FBXW5 interaction (Fig. 2D-E), both the phospho-mimetic SEC23B(S186D) mutant and the endogenous phosphorylated SEC23B interacted with SEC24A, SEC24B, and SEC13 (Supplementary Fig. S2K-L). In addition, both wild-type SEC23B and phospho-mimetic SEC23B(S186D) efficiently bound to the small GTPase SAR1(H79G), a GTP-bound SAR1 mutant that is constitutively associated with COPII vesicles, but not with the cytosolic GDP-bound SAR1(T39N) mutant (Venditti et al., 2012) (Supplementary Fig. S2M).

Altogether, these results indicate that the ULK1-dependent phosphorylation of SEC23B blocks its FBXW5-dependent degradation but does not interfere with either the formation of the SEC23B-SEC24 heterodimer or its recruitment to the COPII vesicle coat by SAR1.

*The FBXW5-mediated degradation of SEC23B limits the autophagic flux in the presence of nutrients*

Since ULK1 plays an essential role in the induction of autophagy, and since COPII proteins, in addition to their role in secretion, are also required for the proper execution of the autophagic program (see Introduction), we investigated whether the ULK1-dependent regulation of the interaction between FBXW5 and SEC23B regulates the autophagic flux. Automated quantification of both endogenous LC3 (Fig. 3A) and exogenous GFP-LC3 (Supplementary Fig. S3A) showed that the LC3 puncta area increased upon FBXW5

downregulation in cells grown in the presence of nutrients. Measurement of area of LC3-positive puncta was preferred to individual number of puncta per cell because clustering of the vesicular compartments in some images made delineation of individual vesicles inaccurate. The increase in LC3-positive puncta could in principle reflect either an increase in autophagic activity or an impairment in the lysosome-dependent degradation of lipidated LC3 (Klionsky et al., 2016). Compared to untreated cells, treatment of FBXW5-depleted cells with bafilomycin A1, a proton ATPase inhibitor that blocks the degradation of lipidated LC3 but not the formation of autophagosomes, significantly increased LC3 puncta (Fig. 3A and Supplementary Fig. S3A), suggesting that depletion of FBXW5 increases autophagic flux during unstressed conditions (*i.e.,* it increases basal autophagy). Consistent with this hypothesis, FBXW5 downregulation did not induce a further increase in the appearance of LC3 puncta upon induction of autophagy by nutrient starvation (Supplementary Fig. S3B).

Next, we used a tandem fluorescent-tagged LC3 construct (mCherry-GFP-LC3) that allows monitoring autophagosome maturation as a change from green+red double (*i.e.,* yellow) florescence vesicles (autophagosomes) to vesicles that fluoresce only in red (autolysosomes) due to GFP-fluorescence quenching at low pH (Klionsky et al., 2016). Using this method, we demonstrated that the majority of LC3 puncta that accumulated upon FBXW5 depletion were autolysosomes and not autophagosomes (Fig. 3B), further confirming that increased levels of SEC23B promotes autophagic flux.

Importantly, co-depletion of SEC23B almost completely prevented the increase in autophagy mediated by FBXW5 silencing (Fig. 3B). Moreover, expression of SEC23B(S186D) significantly induced higher levels of LC3 puncta compared to wild-type SEC23B (Fig. 3C).

*Ser186 in SEC23B is necessary for its localization to the ERGIC and an efficient autophagic response upon nutrient deprivation*

The ERGIC compartment produces vesicles that are active for LC3 lipidation (Egan et al., 2015; Ge et al., 2013; Ge et al., 2014). We found that, whereas upon starvation wild-type SEC23B colocalized approximately twice more with the ERGIC membrane marker ERGIC53, the localization of SEC23B(S186A) did not change after nutrient deprivation (Fig. 3D). Notably, SEC23B(S186D) colocalization with ERGIC53 was already high in the presence of nutrients. Accordingly, compared to wild-type SEC23B, SEC23B(S186D) co-distributed approximately twice more with the ERGIC membrane marker ERGIC53 in fractionated membranes (Supplementary Fig. S3C). Finally, evaluation of the secretory pathway by assaying secreted Gaussia Luciferase (Badr et al., 2007) indicated that overexpression of either SEC23B(S186D) or ULK1, but not wild-type SEC23B, SEC23B(S186A) or ULK1-KD, resulted in an inhibition of secretion in the presence of nutrients, similarly to what observed when cells are staved (Supplementary Fig. S3D-E).

Altogether, these results suggest that ULK1-mediated phosphorylation of SEC23B promotes both its localization to the ERGIC and its autophagic function, possibly to the expense of its secretory function.

Next, we used a CRISPR/Cas9-dependent strategy to generate A375 cells in which all three alleles of *SEC23B* were mutated to SEC23B(S186A) (Supplementary Fig. S3F). In contrast to wild-type SEC23B, levels of SEC23B(S186A) did not increase upon starvation (Fig. 3E). Significantly, automated quantification of endogenous LC3 showed that, in contrast to parental cells, nutrient deprivation-induced autophagy was strongly reduced in

SEC23B(S186A) knock-in cells, while basal autophagy remained unperturbed (Fig. 3F). We also evaluated the turnover of p62, a cargo adaptor and substrate of autophagy (Galluzzi et al., 2018). In response to starvation, p62 was degraded in parental cells but not in SEC23B(S186A) knock-in cells (Fig. 3E).

The above results indicate that the presence of Ser186 in SEC23B and, presumably, its phosphorylation and consequent stabilization are required for the proper induction of autophagy in response to starvation.

*SEC24A/B, but not SEC24C/D, specifically associate with phosphorylated SEC23B and contribute to autophagy*

Vertebrates express four SEC24 paralogs (Fromme et al., 2008), but it is not known whether any of them contribute to the regulation of the autophagic flux. We observed no difference in binding of the phospho-mimetic SEC23B(S186D) mutant with SEC24A and SEC24B (Supplementary Fig. 2K). Because the region of SEC23B that binds FBXW5 and SEC24 proteins overlaps, we investigated whether ULK1-dependent phosphorylation of SEC23B, in addition to blocking its interaction with FBXW5, affects SEC23B association with the other SEC24 paralogs. We observed that whereas both wild-type SEC23B and SEC23B(S186A) associated with all four SEC24 paralogs, SEC23B(S186D) only interacted with SEC24A and SEC24B (Fig. 4A-B). Similarly, SEC24B, but not SEC24C, interacted with endogenous phosphorylated SEC23B (Fig. 4C). Accordingly, molecular dynamics simulations showed that, in contrast to what observed with SEC23B(S186D) and SEC24A, there was a significant loss in the average number of contacts between SEC23B(S186D) and SEC24C, compared to contacts observed with wild-type SEC23B (Supplementary Fig. S4A). We also performed Molecular Mechanics/Generalized Born Surface Area

calculations, which predicted a significantly higher value of binding free energy for the SEC23B(S186D)-SEC24C mutant dimer, resulting in the following trend: SEC23B-SEC24A ~ SEC23B-SEC24C ≲ SEC23B(S186D)-SEC24A << SEC23B(S186D)-SEC24C (Supplementary Fig. S4A). These observations indicate a lack of stability of the SEC23B(S186D)-SEC24C system compared to the other three, in agreement with our experimental results.

Altogether, these results suggest that upon serum starvation, the population of phosphorylated SEC23B preferentially associates with SEC24A and SEC24B.

Notably, co-depletion of both SEC24A and SEC24B, but not SEC24C and SEC24D, inhibited the increase in autophagic flux induced by the silencing of FBXW5 (Fig. 4D and Supplementary Fig. S4B), similar to what we observed by co-depleting SEC23B together with FBXW5 (Fig. 3B). We also evaluated by immunofluorescence the colocalization of SEC24 family members with ERGIC53. Upon starvation, SEC24B, but not SEC24C, colocalized more with ERGIC53 and this event was not observed in SEC23B(S186A) knock-in cells (Supplementary Fig. S4C), suggesting that the localization of SEC24B to the ERGIC is regulated by its association with phospho-SEC23B.

Thus, our data demonstrate the existence of a high degree of specificity among SEC24 paralogs with respect to their ability to contribute to the autophagic flux.

Interestingly, by searching for mutations of SEC23B in publicly available human cancer databases, we found a mutation in melanoma that converts S186 of SEC23B to asparagine (ID#: COSM5391641). We thus generated SEC23B(S186N), a mutant that mimics the cancer associated mutation, and observed a reduced binding to FBXW5, SEC24C, and

SEC24D (Fig. 4E) but not to SEC24A and SEC24B, similar to what observed with SEC23B(S186D) (Fig. 4A). Moreover, SEC23B(S186N) displayed a longer half-life than wild-type SEC23B (Supplementary Fig. S4C). These results suggest that SEC23B(S186N), by being stable, may promote autophagy. To test this hypothesis, we used CRISPR/Cas9 to generate SEC23B(S186N) A375 melanoma cells (Supplementary Fig. S3F). Automated quantification of endogenous LC3 showed that, compared to parental cells, the SEC23B(S186N) knock-in cells displayed more autophagy during unstressed conditions (Fig. 4F). The number of LC3 puncta were also increased in the presence of bafilomycin A1 (Fig. 4F), indicating that SEC23B(S186N) increases the autophagic flux, and that the constitutive increase in LC3 puncta is not due to inhibition of the lysosome-dependent degradation of autophagosomes.

These results show that the SEC23B(S186N) mutation found in melanoma mimics SEC23B phosphorylated on Ser186 similarly to what observed for SEC23B(S186D). In fact, SEC23B(S186N) does not bind efficiently FBXW5, SEC24C, and SEC24D, and promotes autophagy, in agreement with a possible advantageous role resulting from increasing autophagic flux to ensure tumour cell homeostasis (Rybstein et al., 2018).

## DISCUSSION

SEC23B is an essential component of the COPII multi-subunit protein complex that is responsible for the transport of cargo proteins destined to be secreted (Fromme et al., 2008; Zanetti et al., 2011). Although COPII vesicles were originally thought to participate exclusively in the secretory pathway, growing evidence demonstrates that they also play an important role in controlling and executing the autophagic cascade (see Introduction). However, the molecular mechanisms that repurpose COPII for the autophagic process have

remained largely unknown. In this study, we demonstrated that FBXW5 targets SEC23B for degradation to limit autophagy during basal, unperturbed conditions. Upon induction of autophagy by nutrient deprivation, ULK1 phosphorylates Ser186 in SEC23B, inhibiting its interaction with and degradation via FBXW5. The resulting increased levels of SEC23B appear to be crucial for proper autophagic flux. We also found that phosphorylation of Ser186 in SEC23B inhibits its binding to SEC24C and SEC24D, but not SEC24A and SEC24B. Accordingly, depletion of SEC24A and SEC24B, but not SEC24C and SEC24D rescue the phenotype (*i.e.,* the increase in autophagy during non-stressed conditions) induced by FBXW5 silencing. The phosphorylation of Ser186 inhibits the binding of SEC23B to SEC24C and SEC24D, and this may explain, at least in part, the reduced secretion observed upon nutrient starvation.

It has been suggested that autophagic COPII vesicles can be distinguished from trafficking COPII vesicles by their different site of generation, *i.e.,* autophagic COPII vesicles are generated from the ERGIC rather than the ER, and they are potent stimulators of LC3 lipidation in response to starvation (Ge et al., 2015; Ge et al., 2014). PI3KC3, which is activated by ULK1, is required for the relocation of COPII components to the ERGIC (Ge et al., 2015; Ge et al., 2014). However, the differential molecular composition between trafficking COPII vesicles and autophagic COPII vesicles remain largely unknown. PI3KC3, which is activated by ULK1, is required for the relocation of COPII to the ERGIC (Ge et al., 2015; Ge et al., 2014). Our results indicate that autophagic COPII vesicles present at the ERGIC upon starvation contain preferentially SEC23B phosphorylated on Ser186 by ULK1. Moreover, we show that SEC24B, but not SEC24C, colocalizes more abundantly with the ERGIC and this event depends by the presence of Ser186 in SEC23B. Interestingly, in yeast, phosphorylation of Sec24 by casein kinase 1 promotes its binding to autophagy factors to increase autophagosome abundance (Davis et al., 2016), which is reminiscent of what we

found in human cells (*i.e.,* phosphorylation of SEC23B by ULK1 induces the localization of SEC23B and, consequently, SEC24A and SEC24B to the ERGIC to promote the autophagic flux).

Recently, it has been shown that, in presence of nutrients, the basal activity of ULK1 mediates the phosphorylation of SEC16A (promoting the assembly of COPII complexes at the ERES) and that, in response to starvation, the activation of ULK1 induces the dissociation of SEC23A from SEC31A (inhibiting the secretory pathway) (Gan et al., 2017; Joo et al., 2016). Our study shows that, in the absence of nutrients, activated ULK1 promotes the phosphorylation of SEC23B on Ser186 promoting the formation of autophagic COPII vesicles.

Altogether, our results provide evidence for the molecular mechanism by which ULK1 functions as a switch necessary to commit COPII to autophagy in response to starvation (see model in Supplementary Fig. S4D).

## FIGURE LEGENDS

**Figure 1. $SCF^{FBXW5}$ interacts with SEC23B and targets it for ubiquitylation and proteasome-mediated degradation.**

(A) HEK293T cells were transfected with either an empty vector (EV) or the indicated Streptag-FLAG-tagged (SF) F-box proteins (FBPs). Twenty-four hours after transfection, cells were treated with MLN4924 for 4h before harvesting them for affinity-purification (AP) with Streptactin (ST) beads and immunoblotting as indicated. (WCE, whole cell extracts). The white asterisk indicates individual F-box proteins.

(B) HEK293T cells were transfected with an EV, FLAG-HA-tagged FBXW5 (FH-FBXW5), or FH-FBXW5(ΔF) together with SF-tagged SEC23B. Twenty-four hours after transfection, cells were harvested for immunoblotting with the indicated antibodies.

(C) HEK293T cells were transfected with FH-FBXW5 and SF-SEC23B in combination with either an EV, MYC-tagged DN-CUL1, or MYC-tagged DN-CUL4 as indicated. Twenty-four hours after transfection, cells were either left untreated (UT) or treated with MG132 for 6h, and finally harvested for immunoblotting as indicated.

(D) U-2OS cells were transfected with either a non-targeting siRNA oligo (NT) or two different FBXW5 siRNA oligos (individually). Seventy-two hours after siRNA transfection, cells were treated with cycloheximide (CHX) for the indicated times and harvested for immunoblotting. The asterisk indicates a nonspecific band. The graph shows the quantification of SEC23B levels from three independent experiments. Error bars indicate standard deviation.

(E) HEK293T cells were transfected with either an EV or FH-FBXW5. Twenty-four hours after transfection, cells were either left untreated (UT) or treated with MLN4924 for 4h before harvesting them for immunoprecipitation (IP) with FLAG beads and immunoblotting as indicated.

(F) HEK293T cells were transfected with SF-FBXW5 and increasing amounts of HA-tagged SEC24B as indicated. Twenty-four hours after transfection, cells were harvested for affinity-purification (AP) with Streptactin (ST) beads and immunoblotting as indicated.

(G) WCEs from HEK293T cells were incubated with either unconjugated beads or beads coupled to a SEC23B peptide (a.a. 180-194, CEGISKSYVFRGTKD). Beads were washed with lysis buffer and bound proteins were eluted and subjected to SDS-PAGE and immunoblotting.

**Figure 2. ULK1 phosphorylates SEC23B on Serine 186, preventing the FBXW5-dependent degradation of SEC23B.**

(A) HEK293T cells were transfected with either FLAG-tagged SEC23B or FLAG-tagged SEC23B(S186A) in combination with MYC-tagged ULK1 or MYC-tagged ULK1-KD as indicated. Twenty-four hours after transfection, cells were harvested for immunoprecipitation (IP) and immunoblotting. *exo* and *endo* indicate the exogenous and endogenous SEC23B, respectively.

(B) HEK293T cells were transfected with the SF-ULK1 or SF- ULK1-KD as indicated. Twenty-four hours after transfection, cells were treated with various doses of SBI-0206965 (a ULK1-specific inhibitor) for 4 hours before harvesting them for immunoblotting.

(C) HEK293T cells were nutrient-starved with EBSS for the indicated times and harvested for immunoblotting.

(D) HEK293T cells were transfected with EV, SF-SEC23B, or SF-SEC23B mutants. Twenty-four hours after transfection, cells were treated with MLN4924for 4h before harvesting them for affinity-purification (AP) with Streptactin (ST) beads and immunoblotting as indicated.

(E) HEK293T cells were transfected with SF-FBXW5 in combination with either MYC-tagged ULK1 or MYC-tagged ULK1-KD. Twenty-four hours after transfection, cells were treated with MLN4924 for 4h before harvesting them for affinity-purification (AP) with Streptactin (ST) beads and immunoblotting as indicated.

(F) HEK293T cells were transfected with FH-FBXW5 in combination with SF-SEC23B or SF-SEC23B(S186D). Twenty-four hours after transfection, cells were harvested for immunoblotting as indicated.

(G) U-2OS cells stably infected with viruses expressing either SEC23B or SEC23B(S186D) were treated with cycloheximide for the indicated times. The cells were harvested for immunoblotting as indicated.

(H) RPE1-hTERT cells were transfected with siRNAs against the indicated mRNAs. Sixty-eight hours after transfection, cells were nutrient-starved with EBSS for 4 hours and harvested for immunoblotting as indicated. The asterisk indicates the nonspecific band.

**Figure 3. The FBXW5-ULK1-SEC23B nexus controls the autophagic flux.**

(A) RPE1-hTERT cells were transfected with a non-targeting (NT) oligo or a FBXW5-targeting siRNA oligo. Forty-eight hours after transfection, cells were re-plated onto

coverglass for immunofluorescence with an anti-LC3 antibody (left panel). Where indicated, cells were treated with Bafilomycin A1 (BafA1) for 4 hours before fixation. Images of endogenous LC3 puncta underwent automated processing with at least 300 cells counted per sample. Because in several images LC3·puncta were too close to be distinguished, we adopted LC3 puncta area as a criterion for our analysis. The data are presented as mean ± SD (right panel). Scale bar, 10 μm.

(B) U-2OS cells stably expressing tandem fluorescent-tagged LC3 (pBabe-mCherry-EGFP-LC3) were transfected with a NT oligo or a FBXW5 siRNA oligo, alone or in combination with a SEC23B-targeting siRNA oligo as indicated. Forty-eight hours after transfection, cells were replated onto coverglass, followed by fixation twenty-four hours after replating. Images of mCherry-EGFP-LC3 puncta (left panel) underwent automated processing with at least 100 cells counted per sample. The data are presented as mean ± SD (right panel). The yellow and red bars represent green+red double positive LC3 puncta (autophagosome) and red only positive LC3 puncta (autolysosome), respectively. Scale bar, 10 μm.

(C) U-2OS cells were infected with lentiviruses expressing either wild-type SEC23B or SEC23B(S186D). Twenty-four hours after infection, cells were fixed for immunofluorescence (left panel). Images of endogenous LC3 puncta underwent automated processing with at least 300 cells counted per sample. The data are presented as mean ± SD (right panel). Scale bar, 10 μm.

(D) U-2OS cells were transfected with either FLAG-HA-tagged wild-type SEC23B, SEC23B(S186A), or SEC23B(S186D). Twenty-four hours after transfection, cells were fixed for immunofluorescence as indicated (left panels). Images were analysed by ImageJ with at least 100 cells counted per sample. Quantification of SEC23B overlapped with ERGIC53 was performed using the Pearson's correlation coefficient. The data are presented as mean ± SD (right panel). Scale bar, 10 μm.

(E) A375 parental cells or SEC23B(S186A)-A357 knock-in cells were starved with EBSS for the indicated times (+/- BafA1) and harvested for immunoblotting as indicated.

(F) A375 parental cells or SEC23B(S186A)-A357 knock-in cells were starved with EBSS and fixed for immunofluorescence (left panel). Images of endogenous LC3 puncta underwent automated processing with at least 100 cells counted per sample. The data are presented as mean ± SD (right panel). Scale bar, 10 μm.

**Figure 4. Phosphorylated SEC23B interacts with SEC24A and B, which specifically regulate autophagy.**

(A) HEK293T cells were transfected with an EV, SF-SEC23B, or SF-SEC23B mutants. Twenty-four hours after transfection, cells were treated with MLN4924 for 4h before harvesting them for affinity-purification (AP) with Streptactin (ST) beads and immunoblotting as indicated.

(B) HEK293T cells were transfected with an EV or SF) SEC23B(S186D) in combination with either HA-tagged SEC24 paralogs as indicated. Twenty-four hours after transfection, cells were treated with MLN4924 for 4h before harvesting them for immunoprecipitation (IP) with anti-HA beads and immunoblotting as indicated.

(C) HEK293T cells were transfected with either HA-tagged SEC24B or HA-tagged SEC24C together with SF-ULK1. Twenty-four hours after transfection, cells were treated with MLN4924 for 4h before harvesting them for immunoprecipitation (IP) with anti-HA beads and immunoblotting as indicated.

(D) U-2OS cells stably expressing tandem fluorescent-tagged LC3 (pBabe-mCherry-EGFP-LC3) were transfected with a NT oligo or a FBXW5 siRNA oligo in combination with the indicated siRNA oligos. Forty-eight hours after transfection, cells were replated onto coverglass followed by fixation twenty-four hours after replating. Images of mCherry-EGFP-LC3 puncta (left panel) underwent automated processing with at least 100 cells counted per sample. The data are presented as mean ± SD (right panel). Scale bar, 10 μm

(E) HEK239T cells were transfected with either SF-SEC23B or SF-SEC23B(S186N). Twenty-four hours after transfection, cells were harvested for immunoprecipitation (IP) with FLAG-M2 beads and immunoblotted as indicated.

(F) A375 parental cells or SEC23B(S186N)-A357 knock-in cells were treated with BafA1 and fixed for immunofluorescence (left panel). Images of endogenous LC3 puncta underwent automated processing with at least 100 cells counted per sample. The data are presented as mean ± SD (right panel). Scale bar, 10 μm.

**Supplementary Figure S1. FBXW5 interacts with and promotes the degradation of SEC23B.**

(A) HEK293T cells were transfected with Streptag-FLAG-tagged SEC23B (SF-SEC23B) and increasing amounts of FLAG-HA-tagged FBXW5 (FH-FBXW5). Twenty-four hours after transfection, cells were harvested for immunoblotting as indicated.

(B) U-2OS cells stable expressing FLAG-tagged SEC23B were transfected with HA-tagged FBXW5. Twenty-four hours after transfection, cells were fixed with 4% paraformaldehyde in PBS. An anti-FLAG antibody and an anti-HA antibody were used for the detection of SEC23B and FBXW5, respectively. Boxed images were enlarged for clarity.

(C) RPE1-hTERT cells were transfected with either a non-targeting siRNA oligo (NT) or a FBXW5 siRNA oligo. Seventy-two hours after siRNA transfection, cells were treated with cycloheximide (CHX) for the indicated times and harvested for immunoblotting as indicated. The asterisk indicates a nonspecific band.

(D) Schematic view of the SEC23B mutants used in Figure S1H and the SEC23B degron peptide.

(E) HEK293T cells were transfected with the truncated mutants shown in Figure S1G. Twenty-four hours after transfection, cells were harvested for affinity-purification (AP) with Streptactin (ST) beads followed by immunoblotting as indicated. The black asterisk indicates a nonspecific band. The white asterisks indicate bands corresponding to SEC23B or SEC23B mutants.

(F) Crystal structure showing the position of Serine 186 of SEC23. Images (PDB: 3EFO; Mancias and Goldberg, 2008) were created by MolBrowser (Molsoft). The dashed line indicates the interface between SEC23 and SEC24 where serine 186 resides.

**Supplementary Figure S2. Characterization of the phospho-SEC23B (Ser186) antibody and phospho-mimetic SEC23B mutant.**

(A) An ULK1 phosphorylation motif (ΦxxSY/F) (Egan et al., 2015) is highly conserved throughout evolution in the FBXW5-binding region of SEC23B. Φ, hydrophobic amino acids.

(B) Sequence alignment of the previously characterized ULK1-substrates with SEC23B.

(C) A non-phosphorylated SEC23B peptide and an equivalent phospho-peptide (sequences are indicated below the panels) were separated by SDS-PAGE and subjected to immunoblotting either with a phospho-specific SEC23B (Ser186) antibody or with an anti-

SEC23B antibody reactive against both phosphorylated and non-phosphorylated species of SEC23B.

(D) HEK239T cells were transfected with SF- tagged SEC23B or SF-tagged SEC23B mutants. Twenty-four hours after transfection, cells were immunoblotted as indicated.

(E) HEK293T cells were transfected with either FLAG-Streptag-Streptag-tagged SEC23B or FLAG-Streptag-Streptag-tagged SEC23B(S186A) in combination with MYC-tagged ULK1 or MYC-tagged ULK1-KD as indicated. Twenty-four hours after transfection, cells were harvested for immunoblotting as indicated. *exo* and *endo* indicate the exogenous and endogenous SEC23B, respectively.

(F) *In vitro* kinase assays were performed using purified SEC23B (wild-type or the S186A mutant) and ULK1 (wild-type or a kinase-dead mutant) as substrate and kinase, respectively. Purified SEC23B and ULK1 proteins were prepared by immunoprecipitation (followed by elution) from extracts of HEK293T cells transfected with each corresponding plasmid.

(G) HEK293T cells were nutrient-starved with EBSS for the indicated times (plus or minus SBI-0206965, a ULK1-specific inhibitor) and harvested for immunoblotting as indicated.

(H) A non-phosphorylated SEC23B peptide and an equivalent phospho-peptide (sequences are indicated below the panels) were conjugated to beads and used in an *in vitro* binding assay with FBXW5 that was *in vitro* transcribed/translated using a rabbit reticulocyte system. Bound FBXW5 was detected by immunoblotting.

(I) HEK293T cells were transfected with either a Streptag-FLAG empty vector (SF-EV) or Streptag-FLAG-tagged SEC23B (SF-SEC23B). Twenty-four hours after transfection, cells were nutrient-starved with EBSS for the indicated times and treated with MLN4924 for 4h before harvesting them for affinity-purification (AP) with Streptactin (ST) beads and immunoblotting as indicated. (WCE, whole cell extracts). The white asterisk indicates a non-specific band.

(J) RPE1-hTERT cells were transfected as in Figure 2H and harvested for both immunoblotting (Figure 2H) and real-time PCR using ULK2 and GAPDH primers.

(K) HEK239T cells were transfected with either Streptag-FLAG tagged wild-type SEC23B or the phospho-mimetic SEC23B(S186D) mutant (also Streptag-FLAG tagged). Twenty-four hours after transfection, cells were harvested for affinity-purification (AP) with Streptactin (ST) beads and immunoblotting as indicated. (WCE, whole cell extracts).

(L) HEK239T cells were transfected with an empty vector (EV) or HA-tagged SEC24B together with Streptag-FLAG tagged ULK1 (SF-ULK1) as indicated. Twenty-four hours after transfection, cells were harvested for immunoprecipitation (IP) with HA beads and immunoblotting as indicated. (WCE, whole cell extracts).

(M) HEK239T cells were transfected with either Streptag-FLAG tagged SEC23B (SF-SEC23B) or SF-SEC23B(S186D), in combination with the indicated GFP-tagged SAR1 mutants. Twenty-four hours after transfection, cells were harvested for affinity-purification (AP) with Streptactin (ST) beads and immunoblotting as indicated.

**Supplementary Figure S3. FBXW5 controls the autophagic flux and the FBXW5-ULK1-SEC23B nexus controls secretion.**

(A) RPE1-hTERT cells stably expressing GFP-LC3 were transfected with either a non-targeting siRNA oligo (NT) or an siRNA oligo targeting FBXW5 RNA. Forty-eight hours after transfection, cells were replated onto coverglass (left panel). Where indicated, cells were treated with Bafilomycin A1 (BafA1) for 4h before fixation with cold methanol. Images of the GFP-LC3 puncta underwent automated processing with at least 300 cells counted per sample. The data are presented as mean ± SD (right panel). Scale bar, 10 μm.

(B) RPE1-hTERT cells stably expressing GFP-LC3 were transfected with either a non-targeting siRNA oligo (NT) or an siRNA oligo targeting FBXW5 RNA. Forty-eight hours after transfection, cells were replated onto coverglass for immunofluorescence with an anti-LC3 antibody (left panel). Cells were nutrient-starved with EBSS for 4 hours before fixation with cold methanol. Images of the LC3 puncta underwent automated processing with at least 300 cells counted per sample. The data are presented as mean ± SD (right panel). Scale bar, 10 μm.

(C) HeLa cells were permeabilized, incubated with either purified recombinant FLAG-tagged SEC23B or purified recombinant FLAG-tagged SEC23B(S186D), and subjected to subcellular fractionation. Each fraction was subjected to immunoblotting with the indicated antibodies. ERGIC53 was used as a marker of the ERGIC, and RIBOPHORIN-1 as a marker of the ER. SEC23B bands were subjected to densitometry analysis and quantified as percentage of total SEC23B or SEC23B(S186D).

(D) HEK239T cells were transfected with a plasmid expressing Gaussia luciferase in combination with the indicated constructs. Twenty-four hours after transfection, cells were replated onto 96-well plates. After another forty-eight hours, fresh media was added to the cells, and four hours after, the culture media were collected to measure Gaussia

luciferase activity. The data are presented as mean ± SD of the Gaussia luciferase activity of triplicate samples. Expression of FBXW5 was used as a positive control since it results in the downregulation of SEC23B and, therefore, it is expected to inhibit trafficking.

(E) A375 cells stably expressing Gaussia luciferase were plated onto 96-well plates. After forty-eight hours, either fresh media or EBSS was added to the cells and four hours after, the culture media were collected to measure Gaussia luciferase activity. The data are presented as mean ± SD of the Gaussia luciferase activity of triplicate samples.

(F) Schematic representation of the SEC23B genomic locus and gRNA target location. Exon 5 refers to human SEC23B gene (Gene ID: 10483). Wild-type genomic DNA template and knock-in mutant sequences are shown for both SEC23B(S186A) and SEC23B(S186N).

**Supplementary Figure S4. SEC24A and SEC24B, but not SEC24C and SEC24D contribute to the autophagic flux.**

(A) Evolution of the inter-molecular contacts between monomers in the four studied systems during 1 μs molecular dynamics simulations. Left panel: SEC23B-SEC24C (red), SEC23B(S186D)-SEC24C (violet); right panel: SEC23B-SEC24A (red), SEC23B(S186D)-SEC24A (violet). Contacts were calculated as the number of heavy atom interacting pairs within a distance of 4.4Å.

(B) RPE1-hTERT cells were transfected with either a non-targeting oligo (NT) or the siRNA oligos to the indicated mRNAs. Seventy-two hours after transfection, cells were harvested for immunoblotting as indicated.

(C) A375 parental cells or SEC23B(S186D)-A357 knock-in cells were transfected with either HA-tagged SEC24B or HA-tagged SEC24C. Twenty-four hours after transfection, cells were either left untreated (UT) or starved with EBSS for two hours. Next, cells were fixed for immunofluorescence as indicated (upper panel). Images were analysed by ImageJ with at least 100 cells counted per sample. Quantification of SEC24 overlapped with ERGIC53 was performed using the Pearson's correlation coefficient. The data are presented as mean ± SD (bottom panel). Scale bar, 10 μM.

(D) HEK293T cells were transfected with either Streptag-FLAG-tagged (SF) wild-type SEC23B (SF-SEC23B) or Streptag-FLAG-tagged (SF) SEC23B(S186N). Twenty-four hours after transfection, cells were treated with cycloheximide (CHX) for the indicated time and subjected to immunoblot analysis.

(E) Model of how ULK1 and FBXW5 modulate SEC23B-mediated autophagy. See text for details. The SEC23B degron is shown as a red line in SEC23B.

## MATERIAL and METHODS

*Cell lines and drug treatments*

All cells were maintained in DMEM/GlutaMAX supplemented with 10% fetal bovine serum (FBS) and penicillin/streptomycin. For nutrient starvation, DMEM and FBS were removed and cells were grown in EBSS (Sigma) for the indicated times.

*Biochemical methods*

For immunoprecipitation, cell extracts were prepared using lysis buffer (50 mM Tris pH 7.4, 150 mM NaCl, 2 mM EDTA, 10% glycerol, 0.5% NP-40, protease inhibitors, and phosphatase inhibitors), followed by incubation with Streptactin beads (IBA) or FLAG-M2 beads (Sigma) for 2 hours at 4°C. For immunoblotting, each sample was solubilized with lysis buffer (50 mM Tris pH 7.4, 150 mM NaCl, 2 mM EDTA, 10% glycerol, 0.5% NP-40, protease inhibitors, and phosphatase inhibitors). Cell extracts were quantified using BCA protein assay kit (Pierce) and solubilized with LDS-sample buffer (Life technology) followed by boiling at 95℃ for five minutes.

*Immunofluorescence microscopy*

Immunofluorescence microscopy was performed as described previously (Jeong et al., 2013). Briefly, cells were cultured on round coverglass in 24-well culture dishes. After the indicated treatments, cells were washed with PBS followed by fixation with either cold methanol or 4% PFA/PBS. Cells were then permeabilized for 15 minutes with 3% BSA in 0.5% Triton X-100/PBS. Primary antibodies were incubated for one hour at room temperature, and secondary antibodies conjugated to either Alexa Fluor 488 or Alexa Fluor 555 were incubated for one hour at room temperature in 3% BSA/0.1% Triton X-100/PBS. Coverglasses were mounted on slideglass using Pro-long Gold anti-fading reagent with DAPI (Molecular probes).

*Affinity purification and mass spectrometry*

Affinity purification and mass spectrometry were performed as described previously (Jeong et al., 2013). Briefly, Streptag-FLAG-tagged FBXW5 was transiently transfected into HEK293T cells. Cells were treated with MLN4924 for four hours prior to harvest, and then solubilized with lysis buffer (50 mM Tris pH 7.4, 150 mM NaCl, 2 mM EDTA, 10% glycerol, 0.5% NP-40, protease inhibitors, and phosphatase inhibitors). Cell extracts were immunoprecipitated with either Streptactin beads (IBA) or FLAG-M2 beads (Sigma). Immunoprecipitation and subsequent mass spectrometry was carried out as previously described (Kuchay et al., 2017).

*Plasmids, siRNA and shRNA*

FBXW5 and SEC23B mutants were generated using KAPA HiFi polymerase (Kapabiosystems). All cDNAs were subsequently sequenced. ULK1 and ULK1(K46I) plasmids were purchased from Addgene. Sar1 plasmids were generously provided by Dr. Antonella De Matteis. SEC24A, B, C, and D plasmids were generously provided by Dr. Randy Schekman. ON-Target siRNAs targeting FBXW5, SEC23B, SEC24A, SEC24B, SEC24C, SEC24D were purchased from Dharmacon. The production of lentivirus was previously described (Jeong et al., 2013). ULK1 and ULK2 siRNA oligos and pooled FBXW5 siRNA oligos were purchased from Santa Cruz Biotechnology. Non-targeting siRNA oligo (CGUACGCGGAAUACUUCGA) served as a negative control.

*Antibodies*

An anti-FBXW5 antibody was generated by immunizing rabbits with FBXW5 peptides (Yenzyme) and affinity-purified using the same peptides immobilized on CNBr-sepharose. A rabbit polyclonal antibody against phospho-S186-SEC23B was generated and affinity purified by YenZym Antibodies. Anti- SEC23B, SEC24A, SEC24B, SEC24C, and SEC24D antibodies were provided by Dr. Randy Schekman. Mouse monoclonal antibodies were from Sigma-Aldrich (anti-FLAG M2), Covance (anti-HA), and Thermo Scientific (Sar1). Rabbit polyclonal antibodies were from Invitrogen (CUL1 and SKP1), Bethyl Laboratories, Inc. (SEC13 and SEC31A), Cell Signaling Technology (ULK1 and phospho-ULK1 (S757)), Novus Biological (LC3B), Rockland (phospho-ATG13 (S318)), and Abbiotec (phospho-Beclin-1 (S15).

*In vitro kinase assay*

Kinase and substrates were purified from HEK293T cells that had been transfected with plasmids expressing individual kinase and substrates. Kinase reaction buffer (KRB; 20 mM Tris, pH 7.5, 20 mM $MgCl_2$, 25 mM β-glycerophosphate, 2 mM dithiothreitol and 100 μM sodium orthovanadate) were used to elute the purified proteins. Kinase and substrates were mixed and incubated at a final volume of 20 μL in KRB containing 20 μM ATP, 5 μg substrates at 30 °C for 60 min. The reaction was stopped by the addition of sample buffer, boiled and analysed by immunoblot with phospho-SEC23B (Ser186) specific antibody.

*Computational Methods*

The SEC24A and SEC24C monomers were extracted from the Protein Data Bank (PDB) (entries 3EGD and 3EH2, respectively), while SEC23B was modeled by homology from the PDB structure of SEC23A (entry 5KYN), including the missing residues from the crystal structure. The structure of the mutant SEC23B(S186D) was obtained using PyMol Mutagenesis Wizard tool (Edn. Version 1.7. Schrodinger, LLC, 2013). MD simulations were

performed with the GROMACS v5.1 package (Abraham et al., 2015) using the Amber99SB force field (Hornak et al., 2006); the starting conformation for each dimer was modeled from the structure of the SEC23A-SEC24A dimer (PDB 3EGD). Only residues 120 to 405 from SEC23B, 502 to 742 from SEC24, and 173 to 419 from SEC24C were used in the simulations, as these are the domains involved in the dimer interaction, and we have seen that their structures were not influenced by the rest of the protein (data not shown). The systems were solvated with the SPCE water model in a triclinic box, extending at least 10 Å from every atom of the protein, and neutralized adding sufficient Na and Cl counter ions to reach 0.15 M concentration. Bond lengths were constrained using the LINCS algorithm allowing a 2fs time-step. Long-range electrostatics interactions were taken into account using the particle-mesh Ewald (PME) approach. The non-bonded cut-off for Coulomb and Van der Waals interactions were both 10 Å, and the non-bonded pair list was updated every 25 fs. Energy minimization was conducted through the steepest-descent algorithm, until the maximum force decayed to 1000 [kJ $mol^{-1}$ $nm^{-1}$]. The equilibration stage of the whole system consisted in 500 ps of NVT simulation followed by 500 ps of NPT simulation. Temperature was kept constant at 310 K using a modified Berendsen thermostat (Essmann et al., 1995) with a coupling constant of 0.1 ps. Constant pressure of 1 bar was applied in all directions with a coupling constant of 2.0 ps and a compressibility of 4.5 $10^{-5}$ $bar^{-1}$. Finally, the equilibrated systems were subjected to a 1 μs MD simulation run each at 310 K. Binding free energies were calculated using de MM-GBSA scheme (Genheden and Ryde, 2015) provided in the Amber16 package (Case et al., 2017) using the single trajectory approach. Hundred snapshots were collected at time intervals of 5 ns from the last 500 ns of the MD simulations, thus guaranteeing statistical independence (Anisimov and Cavasotto, 2011). The salt concentration was set to 0.150 M, and the dielectric constants to 80 and 1 for the solvent and the proteins, respectively.

*CRISPR genome editing*

To generate SEC23B S186A and S186N knock-in cells, an optimal gRNA target sequence closest to the genomic target site and a 2.1 kb homologous recombination (HR) donor template were designed using the Benchling CRISPR Genome Engineering tool. The HR donor template was designed to introduce alanine or asparagine substitutions at position S186, and a silent mutation to introduce a KpnI restriction site for genotyping. SEC23B gRNA target sequence (see Supplementary Figure S3F) was cloned into pSpCas9(BB)-2A-GFP (PX458), a gift from F. Zhang (Addgene plasmid no. 48138) (Ge et al., 2013). A375 cells were seeded into 10-cm dishes at approximately 70% confluency and transfected

with 2.5 μg each of gRNA-containing PX458 plasmid and HR donor template, using lipofectamine 3000 (Life Technologies). The transfection was performed according to the manufacturer's recommended protocol, using a 2:1 ratio of lipofectamine:DNA. Two days after transfection, GFP-positive cells were sorted using the Beckman Coulter MoFlo XDP cell sorter (100 μm nozzle), and 5,000 cells were plated on a 15-cm dish. About a week later, single-cell clones were picked, trypsinized in 0.25% Trypsin-EDTA for 5 min, and plated into individual wells of a 96-well plate for genotyping. Genomic DNA was collected using QuickExtract (Epicentre). Genotyping PCRs were performed with MyTaq™ HS Red Mix (Bioline), using primers surrounding the genomic target sites. The resulting PCR products were then sequenced and aligned to the corresponding wild-type template in Benchling to determine the presence of a recombination event.

*Gaussia luciferase assay*

To measure the activity of the secretory pathway in HEK293T cells transfected with various cDNAs, a pCMV-*Gaussia* luciferase plasmid (ThermoFisher Scientific) was co-transfected to be used as a reporter by measuring luciferase activity in the conditioned medium (Badr et al., 2007). The activity of the secreted Gaussia luciferase was measured using Pierce Gaussia luciferase Flash Assay Kit (ThermoFisher Scientific) according to the manufacturer's instruction.

*Membrane fractionation*

Membrane fractionation was performed through a modified protocol based on *Ge et al.* (Ge et al., 2013). HeLa cells (ten 15-cm dishes) were cultured to 95% confluence. Cells were treated with 20 μg/ml digitonin (5 min on ice) in B88 (20 mM Hepes, pH 7.2, 250 mM sorbitol, 150 mM potassium acetate, and 5 mM magnesium acetate). Membranes were pelleted at 300xg, washed in B88, and incubated with 3 mM GMPPNP and purified human COPII proteins [10 μg SAR1B and 10 μg of either SEC23B or SEC23B(S186D)], which were purified as described (Kim et al., 2005). Membranes were incubated for 30 min at 37°C and subjected to sequential differential centrifugation at 1,000×*g* (10 min), 3,000×*g* (10 min), 25,000×*g* (20 min) to collect the membranes sedimented at each speed. The 25,000×*g* membrane pellet was suspended in 0.75 ml 1.25 M sucrose buffer and overlayed with 0.5 ml 1.1 M and 0.5 ml 0.25 M sucrose buffer (Golgi isolation kit; Sigma). Centrifugation was performed at 120,000×*g* for 2 hr (TLS 55 rotor, Beckman), after which the interface between 0.25 M and 1.1 M sucrose (L fraction) was selected and suspended in 1 ml 19% OptiPrep for a step gradient containing 0.5 ml 22.5%, 1 ml 19% (sample), 0.9 ml 16%, 0.9 ml 12%, 1 ml 8%, 0.5 ml 5% and 0.2 ml 0% OptiPrep each. Each density of

OptiPrep was prepared by diluting 50% OptiPrep (20 mM Tricine-KOH, pH 7.4, 42 mM sucrose and 1 mM EDTA) with a buffer containing 20 mM Tricine-KOH, pH 7.4, 250 mM sucrose and 1 mM EDTA. The OptiPrep gradient was centrifuged at 150,000×*g* for 3 hr (SW 55 Ti rotor, Beckman) and subsequently fractions of 0.5 ml each, were collected from the top. The fractions were then analyzed by immunoblot.

*Quantification and statistical analysis*

Images were analyzed with an in-house developed python script. Cell counts were calculated by detecting nuclei labeled by DAPI in the blue channel of the image. First, a Gaussian smoothing was applied, and then an Otsu threshold to determine the nuclei mask. This was followed by watershed segmentation to separate touching nuclei, as well as filtering based on area to remove small spots. Partial nuclei touching image borders were included but were counted as a fraction based on the average nuclei size measured in the data set. The puncta (green channel) were detected using the Laplacian of Gaussian (LoG) blob detection algorithm as provided by the python package "scikit-image" (van der Walt et al., 2014). Any blobs found in the regions covered by cell nuclei were ignored. The puncta area was calculated by finding the area of a circle with radius proportional to the standard deviation of the Gaussian kernel that detected the blob, as returned by the LoG algorithm. Prior to applying LoG, some images required a median filter for removal of speckle noise. Some very bright cells were removed from the analysis (identified nuclei and a surrounding area), since it was not possible to distinguish puncta in these areas. These cells were identified by finding outliers from the set of nuclei mean intensities of the image. All statistical analysis was performed with unpaired Student's t test, and it is considered significant when the p value is less than 0.05. n.s., not significant. Data were expressed as mean ± SD of at least three independent experiments performed in triplicate.

## Acknowledgements

The authors thank A. D. Matteis and R. Schekman for reagents; J. Pagan for critical reading the manuscript. M.P. and YT.J. are grateful to T.M. Thor and S.O. Hong, respectively, for continuous support. This work was funded by grants from the National Institute of Health (R01-CA076584 and R01-GM057587) to M.P., and Agencia Nacional de Promoción Científica y Tecnológica-Argentina (PICT-2014-0458, PICT2016-2620) to M.R, and (PICT-2014-3599) to C.N.C. C.N.C. thanks the National System of High Performance Computing (Sistemas Nacionales de Computación de Alto Rendimiento, SNCAD) and the

Computational Centre of High Performance Computing (Centro de Computación de Alto Rendimiento, CeCAR) for granting use of their computational resources. M.P. is an Investigator with the Howard Hughes Medical Institute.

## Author Contributions

YT.J. performed and planned all experiments and helped to write the manuscript. M.P. directed and coordinated the study, designed most experiments, oversaw all results, and co-wrote the manuscript. M.R. supervised the study and co-wrote the manuscript. D.S. helped generating the CRISPR knock-in clones. A.M.C. provided reagents and advices. S.K and D.F performed the automated analysis of the LC3 puncta. D.M. performed membrane fractionation. N.A.S and C.N.C. performed molecular dynamics simulations. A.S., L.F. and M.P.W. performed the mass spectrometry analysis of the protein complexes purified by YT.J. All authors discussed the results and commented on the manuscript.

## REFERENCES

Abraham, M.J., Murtola, T., Schulz, R., Páll, S., Smith, J.C., Hess, B., and Lindahl, E. (2015). GROMACS: High performance molecular simulations through multi-level parallelism from laptops to supercomputers. SoftwareX *1–2*, 19-25.

Anisimov, V.M., and Cavasotto, C.N. (2011). Quantum mechanical binding free energy calculation for phosphopeptide inhibitors of the Lck SH2 domain. Journal of Computational Chemistry *32*, 2254–2263.

Badr, C.E., Hewett, J.W., Breakefield, X.O., and Tannous, B.A. (2007). A highly sensitive assay for monitoring the secretory pathway and ER stress. PLoS One *2*, e571.

Boyadjiev, S.A., Fromme, J.C., Ben, J., Chong, S.S., Nauta, C., Hur, D.J., Zhang, G., Hamamoto, S., Schekman, R., Ravazzola, M., *et al.* (2006). Cranio-lenticulo-sutural dysplasia is caused by a SEC23A mutation leading to abnormal endoplasmic-reticulum-to-Golgi trafficking. Nat Genet *38*, 1192-1197.

Case, D.A., Cerutti, T.E., Cheatham, T.E.I., Darden, T.A., Duke, R.E., Giese, T.J., Gohlke, H., Goetz, A.W., Greene, D., Homeyer, N., *et al.* (2017). AMBER 2017. (San Francisco, University of California).

Dankert, J.F., Rona, G., Clijsters, L., Geter, P., Skaar, J.R., Bermudez-Hernandez, K., Sassani, E., Fenyo, D., Ueberheide, B., Schneider, R., *et al.* (2016). Cyclin F-Mediated Degradation of SLBP Limits H2A.X Accumulation and Apoptosis upon Genotoxic Stress in G2. Mol Cell *64*, 507-519.

Davis, S., Wang, J., and Ferro-Novick, S. (2017). Crosstalk between the Secretory and Autophagy Pathways Regulates Autophagosome Formation. Dev Cell *41*, 23-32.

Davis, S., Wang, J., Zhu, M., Stahmer, K., Lakshminarayan, R., Ghassemian, M., Jiang, Y., Miller, E.A., and Ferro-Novick, S. (2016). Sec24 phosphorylation regulates autophagosome abundance during nutrient deprivation. Elife *5*.

Egan, D.F., Chun, M.G., Vamos, M., Zou, H., Rong, J., Miller, C.J., Lou, H.J., Raveendra-Panickar, D., Yang, C.C., Sheffler, D.J., *et al.* (2015). Small Molecule Inhibition of the Autophagy Kinase ULK1 and Identification of ULK1 Substrates. Mol Cell *59*, 285-297.

Essmann, U., Perera, L., Berkowitz, M.L., Darden, T., Lee, H., and Pedersen, L.G. (1995). A smooth particle mesh Ewald method. Journal of Chemical Physics *103*, 8577-8593.

Florens, L., and Washburn, M.P. (2006). Proteomic analysis by multidimensional protein identification technology. Methods Mol Biol *328*, 159-175.

Frescas, D., and Pagano, M. (2008). Deregulated proteolysis by the F-box proteins SKP2 and beta-TrCP: tipping the scales of cancer. Nat Rev Cancer *8*, 438-449.

Fromme, J.C., Orci, L., and Schekman, R. (2008). Coordination of COPII vesicle trafficking by Sec23. Trends Cell Biol *18*, 330-336.

Galluzzi, L., Vitale, I., Aaronson, S.A., Abrams, J.M., Adam, D., Agostinis, P., Alnemri, E.S., Altucci, L., Amelio, I., Andrews, D.W.*, et al.* (2018). Molecular mechanisms of cell death: recommendations of the Nomenclature Committee on Cell Death 2018. Cell Death Differ *25*, 486-541.

Gan, W., Zhang, C., Siu, K.Y., Satoh, A., Tanner, J.A., and Yu, S. (2017). ULK1 phosphorylates Sec23A and mediates autophagy-induced inhibition of ER-to-Golgi traffic. BMC Cell Biol *18*, 22.

Ge, L., Melville, D., Zhang, M., and Schekman, R. (2013). The ER-Golgi intermediate compartment is a key membrane source for the LC3 lipidation step of autophagosome biogenesis. Elife *2*, e00947.

Ge, L., Wilz, L., and Schekman, R. (2015). Biogenesis of autophagosomal precursors for LC3 lipidation from the ER-Golgi intermediate compartment. Autophagy *11*, 2372-2374.

Ge, L., Zhang, M., Kenny, S.J., Liu, D., Maeda, M., Saito, K., Mathur, A., Xu, K., and Schekman, R. (2017). Remodeling of ER-exit sites initiates a membrane supply pathway for autophagosome biogenesis. EMBO Rep *18*, 1586-1603.

Ge, L., Zhang, M., and Schekman, R. (2014). Phosphatidylinositol 3-kinase and COPII generate LC3 lipidation vesicles from the ER-Golgi intermediate compartment. Elife *3*, e04135.

Genheden, S., and Ryde, U. (2015). The MM/PBSA and MM/GBSA methods to estimate ligand-binding affinities. Expert Opin Drug Discov *10*, 449-461.

Hornak, V., Abel, R., Okur, A., Strockbine, B., Roitberg, A., and Simmerling, C. (2006). Comparison of multiple Amber force fields and development of improved protein backbone parameters. Proteins *65*, 712-725.

Hurley, J.H., and Young, L.N. (2017). Mechanisms of Autophagy Initiation. Annu Rev Biochem *86*, 225-244.

Ishihara, N., Hamasaki, M., Yokota, S., Suzuki, K., Kamada, Y., Kihara, A., Yoshimori, T., Noda, T., and Ohsumi, Y. (2001). Autophagosome requires specific early Sec proteins for its formation and NSF/SNARE for vacuolar fusion. Mol Biol Cell *12*, 3690-3702.

Jeong, Y.T., Rossi, M., Cermak, L., Saraf, A., Florens, L., Washburn, M.P., Sung, P., Schildkraut, C.L., and Pagano, M. (2013). FBH1 promotes DNA double-strand breakage and apoptosis in response to DNA replication stress. J Cell Biol *200*, 141-149.

Jiang, P., and Mizushima, N. (2014). Autophagy and human diseases. Cell Res *24*, 69-79.

Joo, J.H., Wang, B., Frankel, E., Ge, L., Xu, L., Iyengar, R., Li-Harms, X., Wright, C., Shaw, T.I., Lindsten, T.*, et al.* (2016). The Noncanonical Role of ULK/ATG1 in ER-to-Golgi Trafficking Is Essential for Cellular Homeostasis. Mol Cell *62*, 982.

Karanasios, E., Walker, S.A., Okkenhaug, H., Manifava, M., Hummel, E., Zimmermann, H., Ahmed, Q., Domart, M.C., Collinson, L., and Ktistakis, N.T. (2016). Autophagy initiation by ULK complex assembly on ER tubulovesicular regions marked by ATG9 vesicles. Nat Commun *7*, 12420.

Kim, J., Hamamoto, S., Ravazzola, M., Orci, L., and Schekman, R. (2005). Uncoupled packaging of amyloid precursor protein and presenilin 1 into coat protein complex II vesicles. J Biol Chem *280*, 7758-7768.

Kim, T.Y., Jackson, S., Xiong, Y., Whitsett, T.G., Lobello, J.R., Weiss, G.J., Tran, N.L., Bang, Y.J., and Der, C.J. (2013). CRL4A-FBXW5-mediated degradation of DLC1 Rho GTPase-activating protein tumor suppressor promotes non-small cell lung cancer cell growth. Proc Natl Acad Sci U S A *110*, 16868-16873.

Klionsky, D.J., Abdelmohsen, K., Abe, A., Abedin, M.J., Abeliovich, H., Acevedo Arozena, A., Adachi, H., Adams, C.M., Adams, P.D., Adeli, K.*, et al.* (2016). Guidelines for the use and interpretation of assays for monitoring autophagy (3rd edition). Autophagy *12*, 1-222.

Kuchay, S., Giorgi, C., Simoneschi, D., Pagan, J., Missiroli, S., Saraf, A., Florens, L., Washburn, M.P., Collazo-Lorduy, A., Castillo-Martin, M.*, et al.* (2017). PTEN counteracts FBXL2 to promote IP3R3- and Ca(2+)-mediated apoptosis limiting tumour growth. Nature *546*, 554-558.

Lamb, C.A., Yoshimori, T., and Tooze, S.A. (2013). The autophagosome: origins unknown, biogenesis complex. Nat Rev Mol Cell Biol *14*, 759-774.

Lang, M.R., Lapierre, L.A., Frotscher, M., Goldenring, J.R., and Knapik, E.W. (2006). Secretory COPII coat component Sec23a is essential for craniofacial chondrocyte maturation. Nat Genet *38*, 1198-1203.

Lemus, L., Ribas, J.L., Sikorska, N., and Goder, V. (2016). An ER-Localized SNARE Protein Is Exported in Specific COPII Vesicles for Autophagosome Biogenesis. Cell Rep *14*, 1710-1722.

Mancias, J.D., and Goldberg, J. (2007). The transport signal on Sec22 for packaging into COPII-coated vesicles is a conformational epitope. Mol Cell *26*, 403-414.

Mizushima, N. (2010). The role of the Atg1/ULK1 complex in autophagy regulation. Curr Opin Cell Biol *22*, 132-139.

Mizushima, N., Yoshimori, T., and Ohsumi, Y. (2011). The role of Atg proteins in autophagosome formation. Annu Rev Cell Dev Biol *27*, 107-132.

Petroski, M.D., and Deshaies, R.J. (2005). Function and regulation of cullin-RING ubiquitin ligases. Nat Rev Mol Cell Biol *6*, 9-20.

Reggiori, F., Wang, C.W., Nair, U., Shintani, T., Abeliovich, H., and Klionsky, D.J. (2004). Early stages of the secretory pathway, but not endosomes, are required for Cvt vesicle and autophagosome assembly in Saccharomyces cerevisiae. Mol Biol Cell *15*, 2189-2204.

Rybstein, M.D., Bravo-San Pedro, J.M., Kroemer, G., and Galluzzi, L. (2018). The autophagic network and cancer. Nat Cell Biol *20*, 243-251.

Sanchez-Wandelmer, J., Ktistakis, N.T., and Reggiori, F. (2015). ERES: sites for autophagosome biogenesis and maturation? J Cell Sci *128*, 185-192.

Schwarz, K., Iolascon, A., Verissimo, F., Trede, N.S., Horsley, W., Chen, W., Paw, B.H., Hopfner, K.P., Holzmann, K., Russo, R., *et al.* (2009). Mutations affecting the secretory COPII coat component SEC23B cause congenital dyserythropoietic anemia type II. Nat Genet *41*, 936-940.

Skaar, J.R., Pagan, J.K., and Pagano, M. (2013). Mechanisms and function of substrate recruitment by F-box proteins. Nat Rev Mol Cell Biol *14*, 369-381.

Skaar, J.R., Pagan, J.K., and Pagano, M. (2014). SCF ubiquitin ligase-targeted therapies. Nat Rev Drug Discov *13*, 889-903.

Stadel, D., Millarte, V., Tillmann, K.D., Huber, J., Tamin-Yecheskel, B.C., Akutsu, M., Demishtein, A., Ben-Zeev, B., Anikster, Y., Perez, F., *et al.* (2015). TECPR2 Cooperates with LC3C to Regulate COPII-Dependent ER Export. Mol Cell *60*, 89-104.

Tan, D., Cai, Y., Wang, J., Zhang, J., Menon, S., Chou, H.T., Ferro-Novick, S., Reinisch, K.M., and Walz, T. (2013). The EM structure of the TRAPPIII complex leads to the identification of a requirement for COPII vesicles on the macroautophagy pathway. Proc Natl Acad Sci U S A *110*, 19432-19437.

van der Walt, S., Schonberger, J.L., Nunez-Iglesias, J., Boulogne, F., Warner, J.D., Yager, N., Gouillart, E., and Yu, T. (2014). scikit-image: image processing in Python. PeerJ *2*, e453.

Venditti, R., Scanu, T., Santoro, M., Di Tullio, G., Spaar, A., Gaibisso, R., Beznoussenko, G.V., Mironov, A.A., Mironov, A., Jr., Zelante, L., *et al.* (2012). Sedlin controls the ER export of procollagen by regulating the Sar1 cycle. Science *337*, 1668-1672.

Wang, J., Tan, D., Cai, Y., Reinisch, K.M., Walz, T., and Ferro-Novick, S. (2014). A requirement for ER-derived COPII vesicles in phagophore initiation. Autophagy *10*, 708-709.

Zacharogianni, M., Aguilera-Gomez, A., Veenendaal, T., Smout, J., and Rabouille, C. (2014). A stress assembly that confers cell viability by preserving ERES components during amino-acid starvation. Elife *3*.

Zacharogianni, M., Kondylis, V., Tang, Y., Farhan, H., Xanthakis, D., Fuchs, F., Boutros, M., and Rabouille, C. (2011). ERK7 is a negative regulator of protein secretion in response to amino-acid starvation by modulating Sec16 membrane association. EMBO J *30*, 3684-3700.

Zanetti, G., Pahuja, K.B., Studer, S., Shim, S., and Schekman, R. (2011). COPII and the regulation of protein sorting in mammals. Nat Cell Biol *14*, 20-28.

Zoppino, F.C., Militello, R.D., Slavin, I., Alvarez, C., and Colombo, M.I. (2010). Autophagosome formation depends on the small GTPase Rab1 and functional ER exit sites. Traffic *11*, 1246-1261.

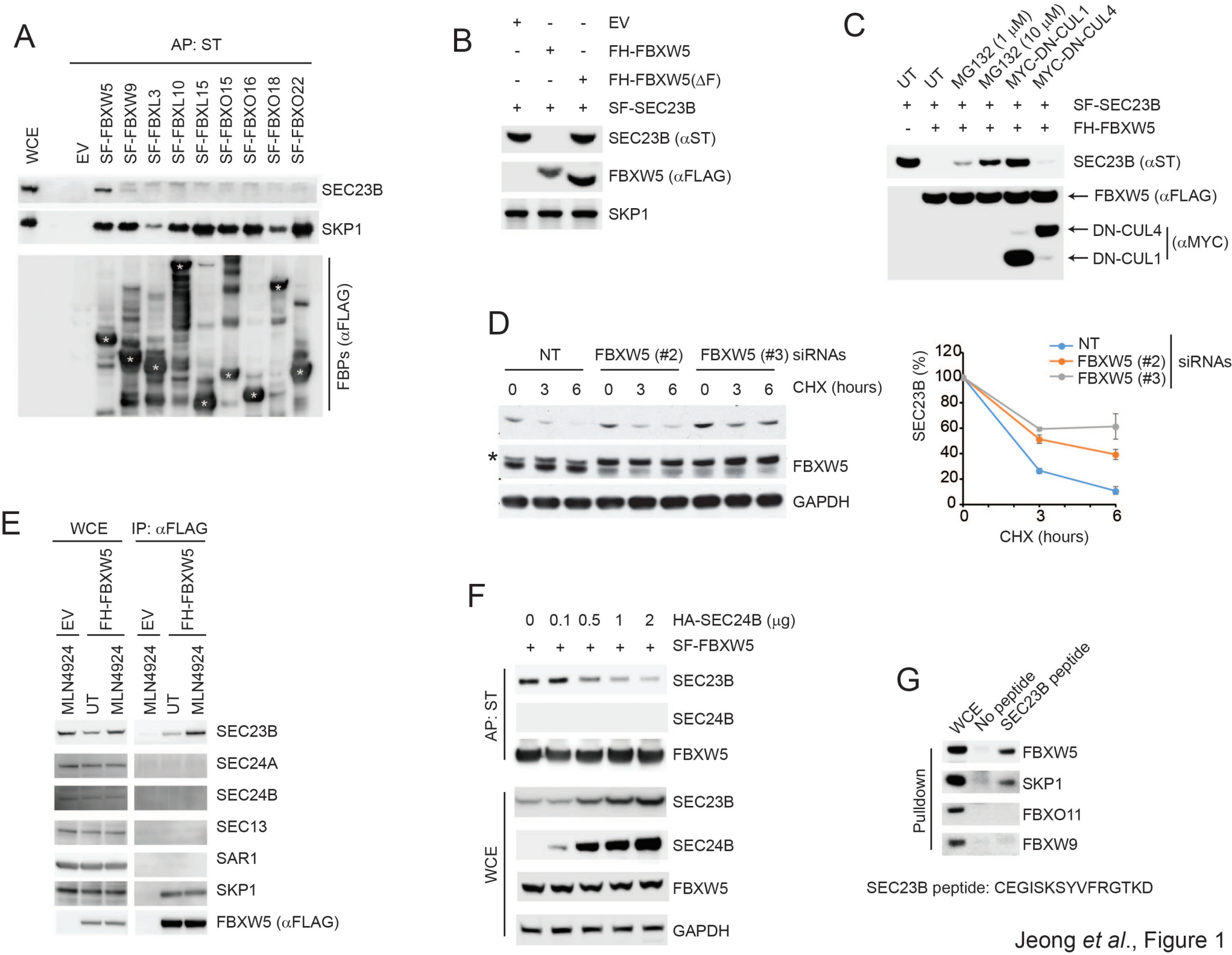
A
AP: ST
WCE
EV
SF-FBXW5
SF-FBXW9
SF-FBXL3
SF-FBXL10
SF-FBXL15
SF-FBXO15
SF-FBXO16
SF-FBXO18
SF-FBXO22
SEC23B
SKP1
FBPs (αFLAG)
B
EV
FH-FBXW5
FH-FBXW5(ΔF)
SF-SEC23B
SEC23B (αST)
FBXW5 (αFLAG)
SKP1
C
UT
UT
MG132 (1 μM)
MG132 (10 μM)
MYC-DN-CUL1
MYC-DN-CUL4
SF-SEC23B
FH-FBXW5
SEC23B (αST)
FBXW5 (αFLAG)
DN-CUL4
DN-CUL1
(αMYC)
D
NT
FBXW5 (#2)
FBXW5 (#3)
siRNAs
0 3 6 0 3 6 0 3 6
CHX (hours)
FBXW5
GAPDH
SEC23B (%)
120
100
80
60
40
20
0
0 3 6
CHX (hours)
NT
FBXW5 (#2)
FBXW5 (#3)
siRNAs
E
WCE
IP: αFLAG
EV
FH-FBXW5
EV
FH-FBXW5
MLN4924
UT
MLN4924
MLN4924
UT
MLN4924
SEC23B
SEC24A
SEC24B
SEC13
SAR1
SKP1
FBXW5 (αFLAG)
F
0 0.1 0.5 1 2 HA-SEC24B (μg)
SF-FBXW5
AP: ST
SEC23B
SEC24B
FBXW5
WCE
SEC23B
SEC24B
FBXW5
GAPDH
G
WCE
No peptide
SEC23B peptide
Pulldown
FBXW5
SKP1
FBXO11
FBXW9
SEC23B peptide: CEGISKSYVFRGTKD
Jeong et al., Figure 1

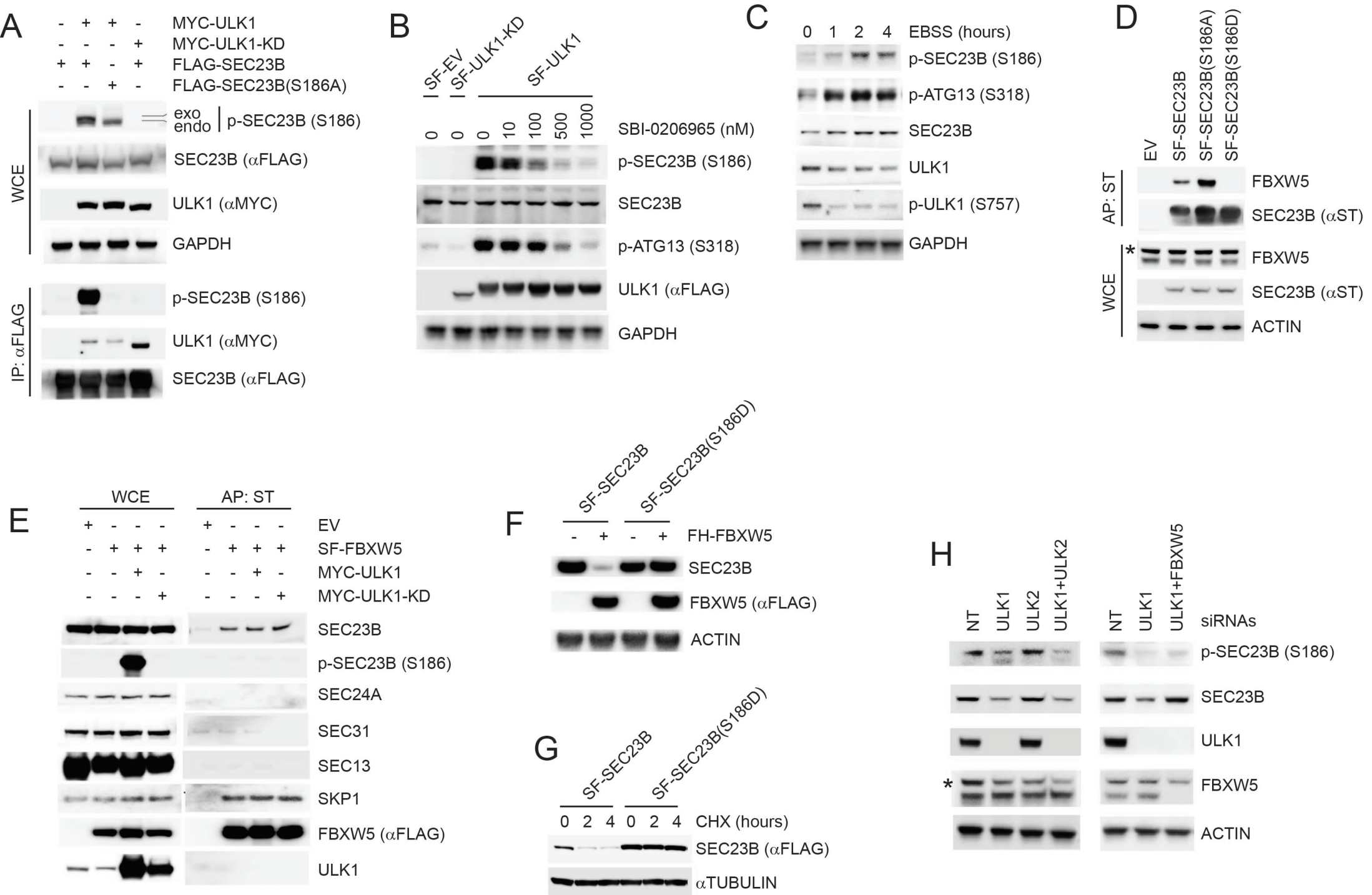


Jeong *et al.*, Figure 2

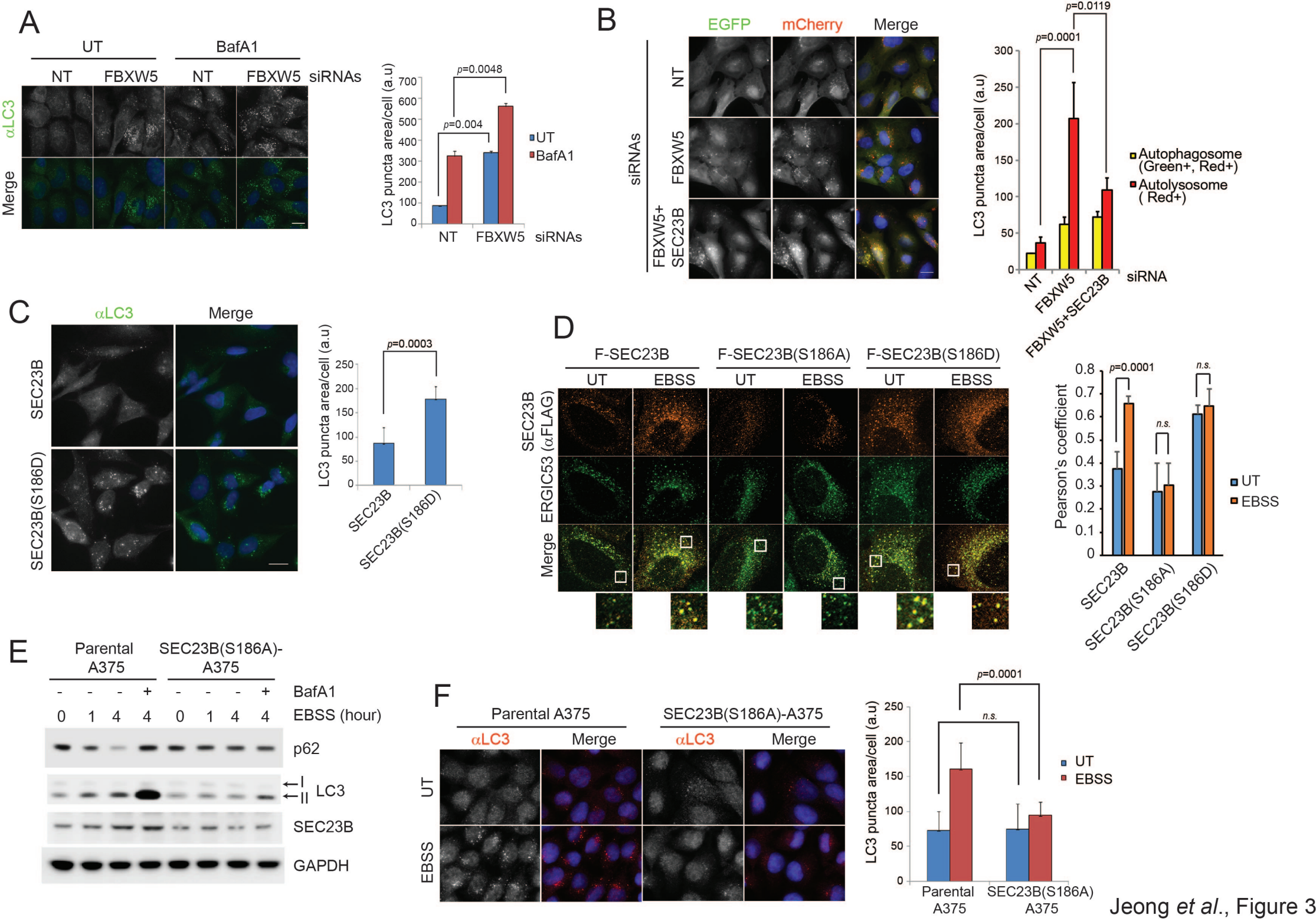


Jeong *et al.*, Figure 3

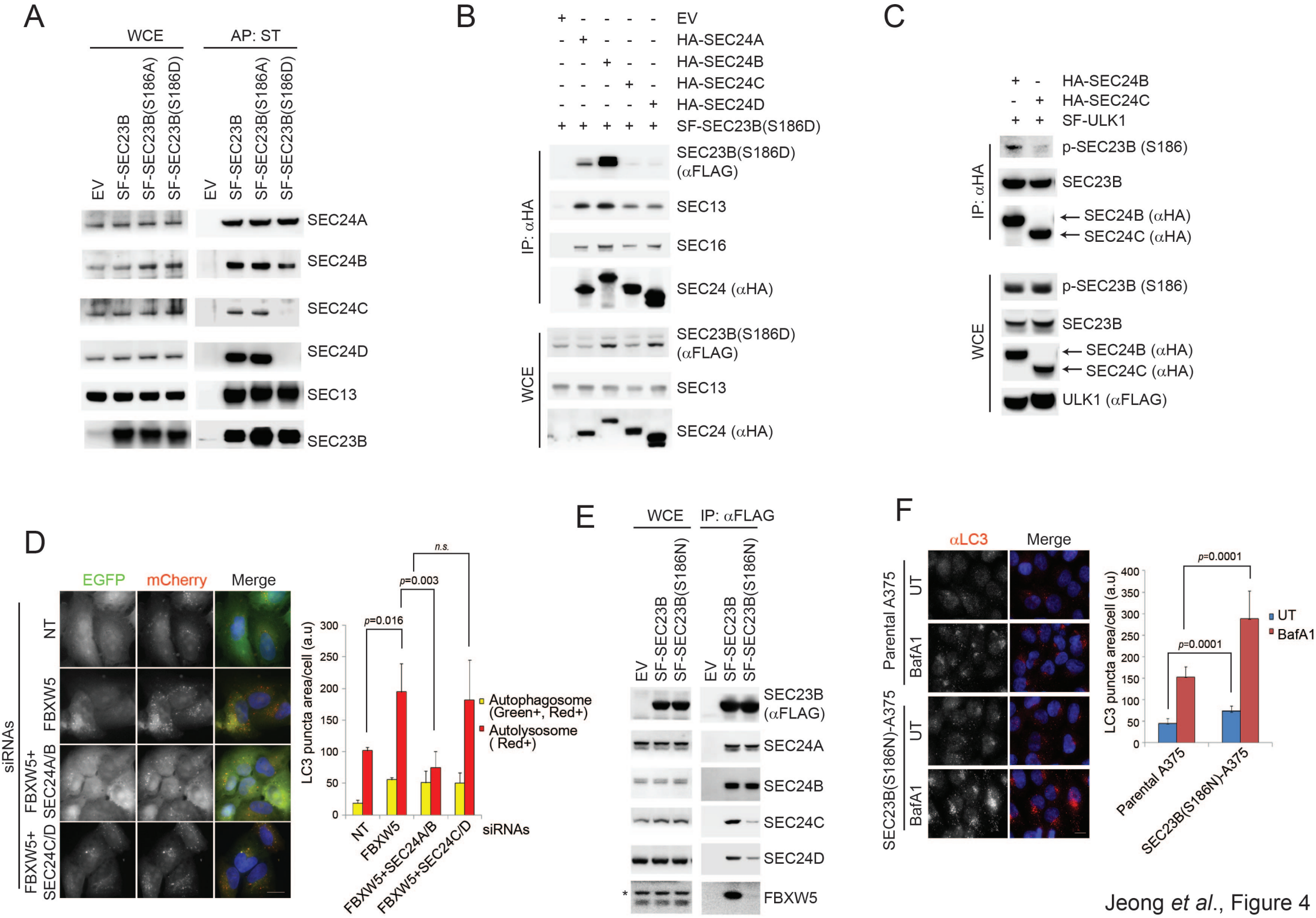


Jeong *et al.*, Figure 4

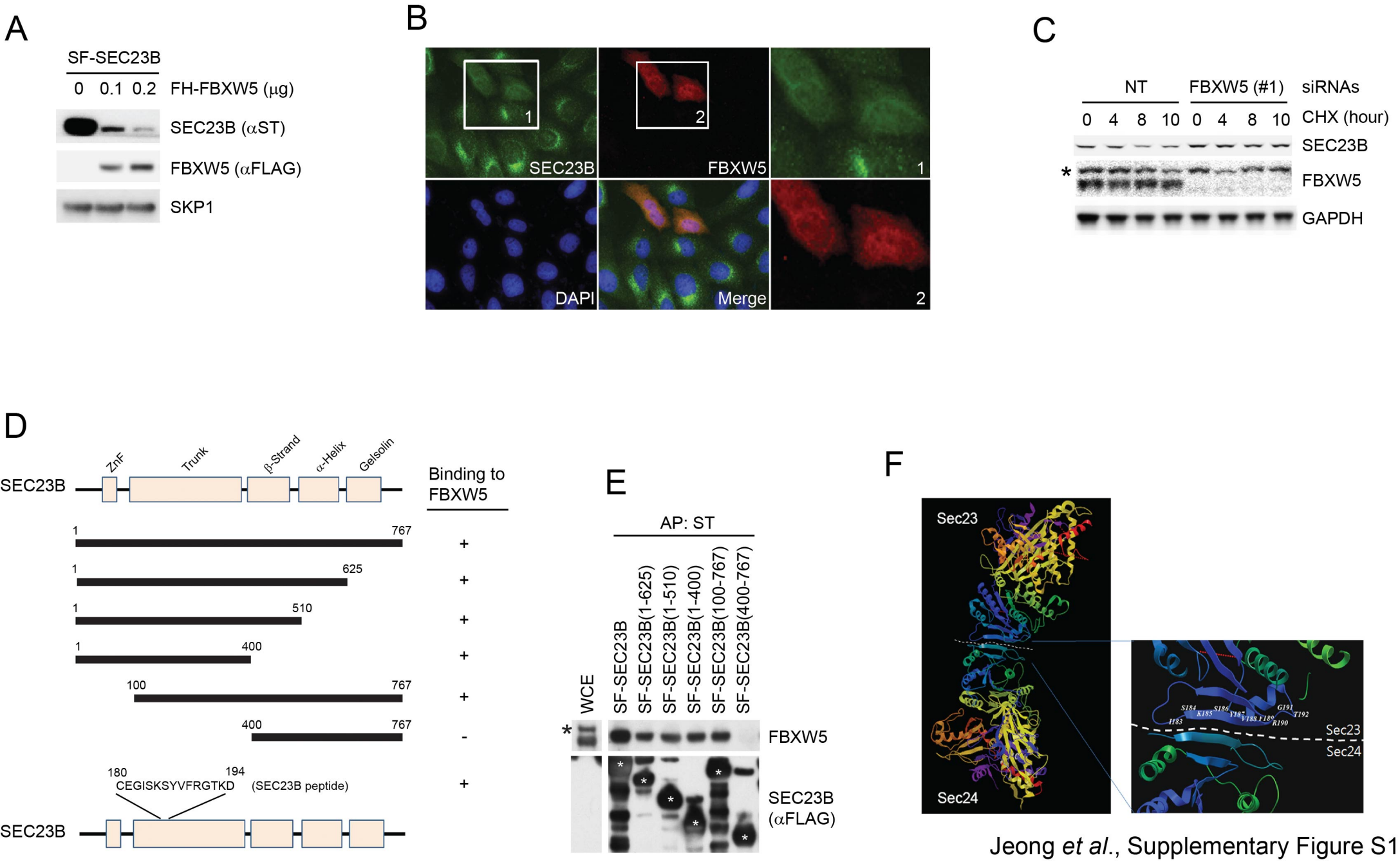


Jeong *et al.*, Supplementary Figure S1

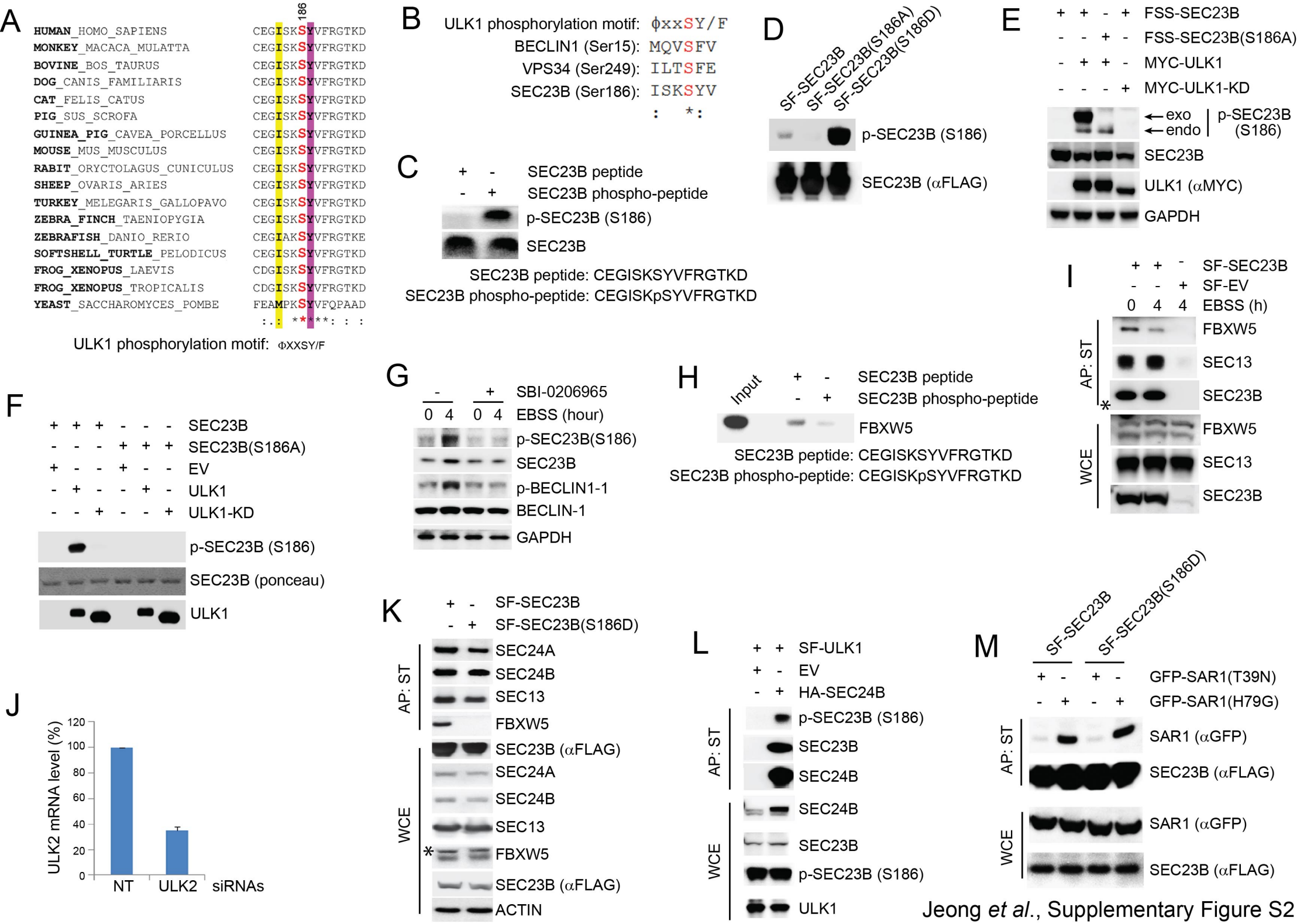


Jeong *et al.*, Supplementary Figure S2

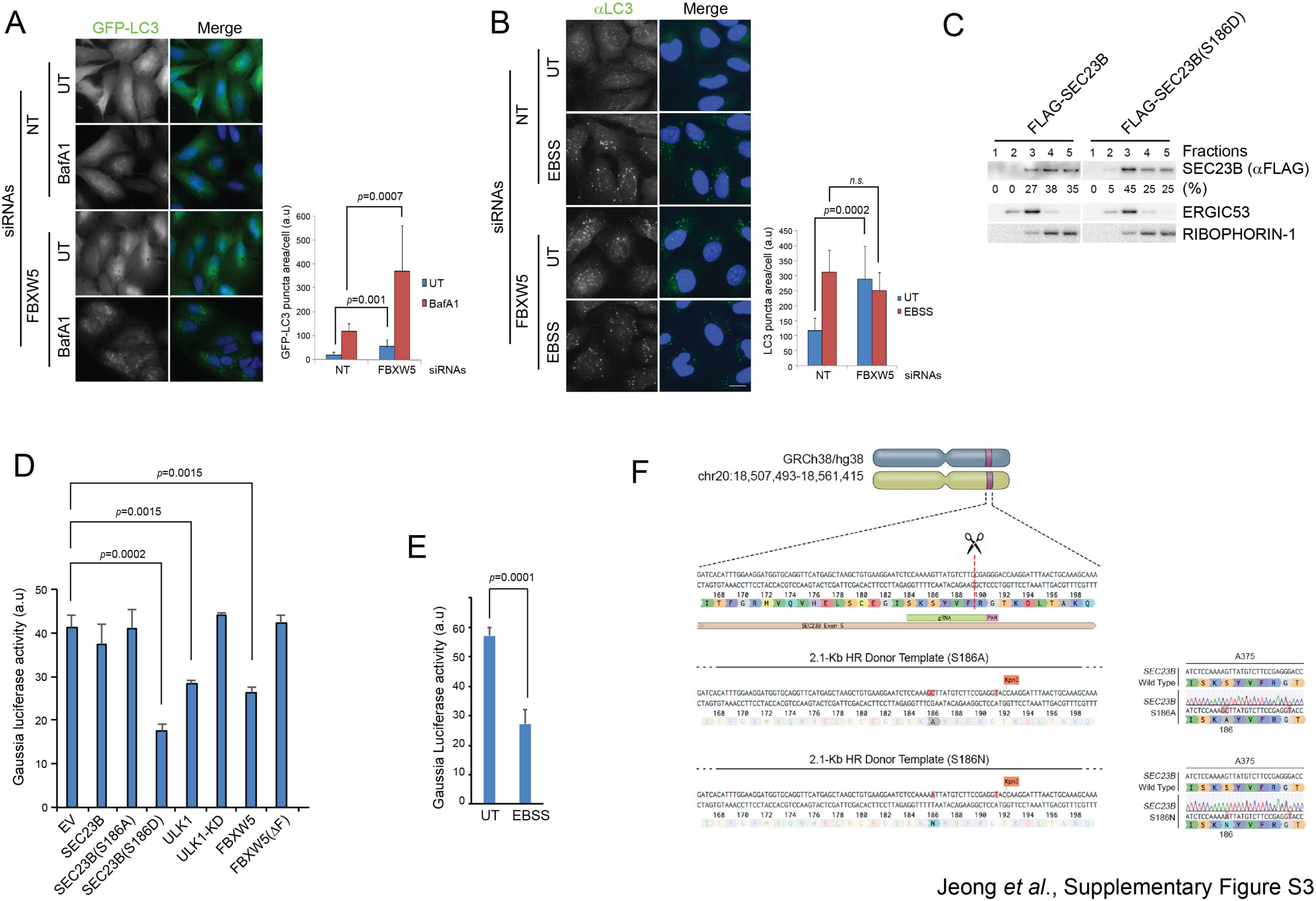


Jeong *et al.*, Supplementary Figure S3

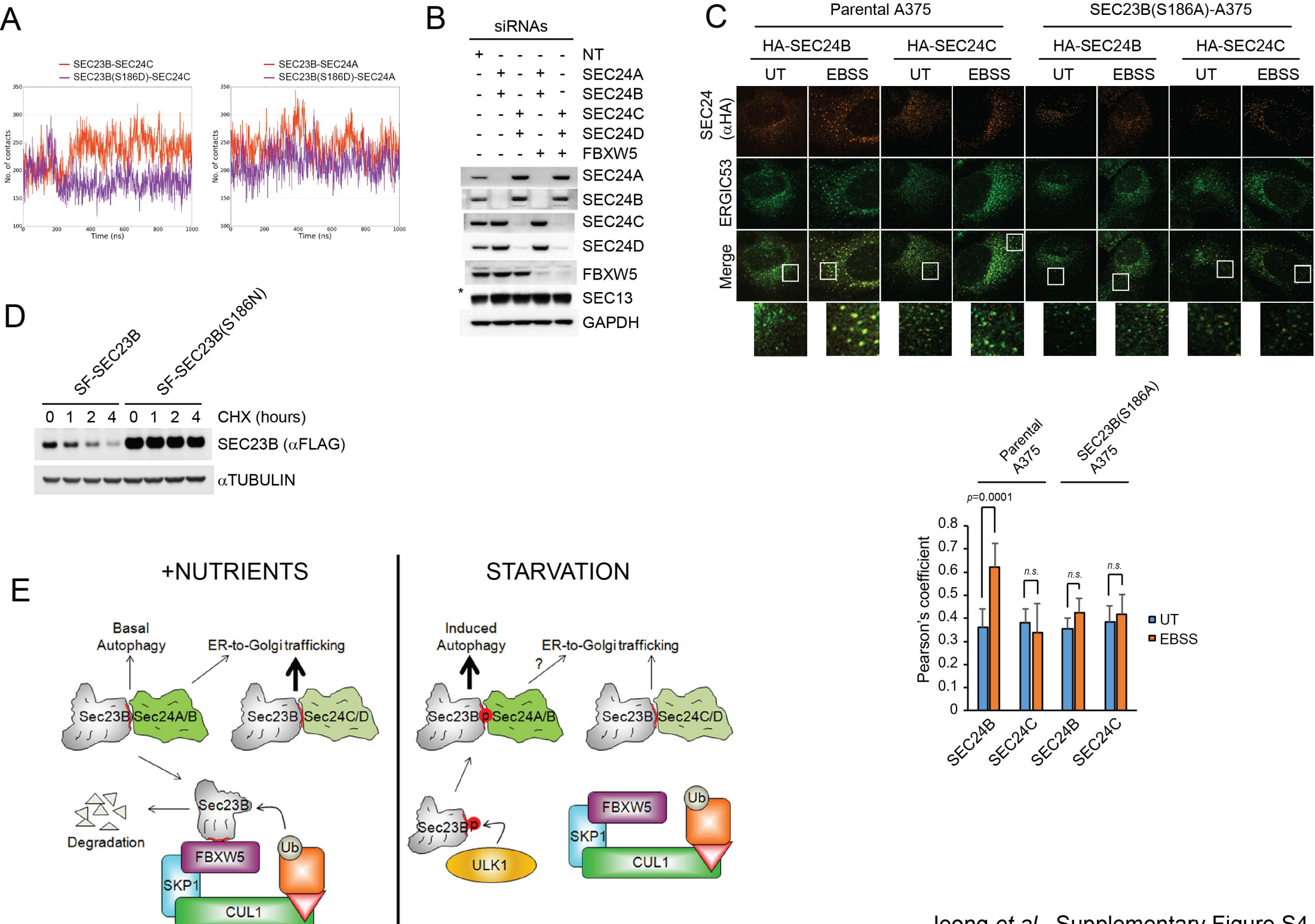


Jeong *et al.*, Supplementary Figure S4